The geometrical shape of mesenchymal stromal cells measured by quantitative shape descriptors is determined by the stiffness of the biomaterial and by cyclic tensile forces

[1,$] Tatiana Uynuk-Ool, [1,$] Miriam Rothdiener, [2] Brandan Walters, [3] Miriam Hegemann, [1] Julian Palm, [1] Phong Nguyen, [4] Tanja Seeger, [5] Ulrich Stöckle, [2] Jan P. Stegemann, [3] Wilhelm K. Aicher, [6] Bodo Kurz, [1] Melanie L. Hart, [4] Gerd Klein, [1] Bernd Rolauffs*

[$]Shared first authorship

[1] Siegfried Weller Institute for Trauma Research, BG Trauma Clinic Tuebingen, University of Tuebingen, Waldhoernlestr. 22, 72072 Tuebingen, Germany

[2] Department of Biomedical Engineering, University of Michigan, 1107 Carl A. Gerstacker Building, 2200 Bonisteel Blvd, Ann Arbor, MI 48109, United States

[3] Department of Urology, University of Tuebingen, Hoppe-Seyler-Straße 3, 72076 Tuebingen, Germany

[4] University Medical Clinic, Department II, Center for Medical Research, University of Tuebingen, Waldhoernlestr. 22, 72072 Tuebingen, Germany

[5] Clinic for Trauma and Restorative Surgery, BG Trauma Clinic Tuebingen, University of Tuebingen, Schnarrenberstr. 95, 72076 Tuebingen, Germany

[6] Department of Anatomy, Christian-Albrechts-University, Otto-Hahn-Platz 8, 24118 Kiel, Germany

Running head: Quantitative shape descriptors for mesenchymal stromal cell morphology

* To whom correspondence should be addressed:

Bernd Rolauffs, M.D., BG Trauma Clinic Tuebingen, Schnarrenbergstr 95, 72076 Tuebingen, Germany; Phone: +49-7071-6060; Email: berndrolauffs@googlemail.com

This is the author manuscript accepted for publication and has undergone full peer review but has not been through the copyediting, typesetting, pagination and proofreading process, which may lead to differences between this version and the Version of Record. Please cite this article as doi: 10.1002/term.2263

Support: This work was funded in part by the German Research Council (RO2511/3-1 to B.R.; KL709/13-1 to G.K.; AL16/23-1 to W.K.A.), and the intramural financial and personnel support of the BG Trauma Clinic Tuebingen (Berufsgenossenschaftliche Unfallklinik Tuebingen) and the clinic operator Heidelberg Association for the Treatment of Occupational Injuries (Verein für Berufsgenossenschaftliche Heilbehandlung Heidelberg e.V.).

Abstract

Controlling mesenchymal stromal cell (MSC) shape is a novel method for investigating and directing MSC behavior *in vitro*. We hypothesized that specific MSC shapes can be generated by using stiffness-defined biomaterial surfaces and by applying cyclic tensile forces. Biomaterials used were thin and thick silicone sheets, fibronectin coating, and compacted collagen type I sheets. MSC morphology was quantified by shape descriptors describing dimensions and membrane protrusions. Nanoscale stiffness was measured by atomic force microscopy and the expression of smooth muscle cell (SMC) marker genes (*ACTA2, TAGLN, CNN1*) by quantitative RT-PCR. Cyclic stretch was applied with 2.5 % or 5 % amplitudes. Attachment to biomaterials with a higher stiffness yielded more elongated MSCs with less membrane protrusions, compared to biomaterials with a lower stiffness. For cyclic stretch, we selected compacted collagen sheets, which were associated with the most elongated MSC shape across all investigated biomaterials. Cyclic stretch elongated MSCs during stretch as expected. One hour after cessation of stretch, however, MSC shape was rounder again, suggesting loss of stretch-induced shape. Different shape descriptor values obtained by different stretch regimes correlated significantly with the expression levels of SMC marker genes. Values of approximately 0.4 for roundness and 3.4 for aspect ratio were critical for the highest expression levels of *ACTA2* and *CNN1*. Thus, specific shape descriptor values, which can be generated using biomaterial-associated stiffness and tensile forces, can serve as a template for the induction of specific gene expression levels in MSC.

Keywords: mesenchymal stromal cell; MSC; shape; shape descriptor; compacted collagen; cyclic stretch; roundness; aspect ratio; circularity; solidity; nanoscale stiffness; myogenic differentiation; biomaterial; silicone

1 Introduction

The shape of cells is a fundamental signal for proliferation (Singhvi R *et al.* 1994), a potent regulator of cell growth and physiology, and is adapted for specific functions (Folkman J and Moscona A 1978). During embryonic development and tissue regeneration, many events are initiated to change stem cell shape, and this change in shape can influence tissue structure and function (Manasek FJ *et al.* 1972, Yang Y *et al.* 1999). Mesenchymal stromal cells (MSCs) can differentiate *in vitro* into cell types of mesodermal origin including osteogenic, chondrogenic, adipogenic and myogenic lineages (Caplan AI 2007, Aicher WK *et al.* 2011, Klein G *et al.* 2015). To control MSC differentiation via controlling cellular shape, previous studies have generated dynamically elongated shape using cyclic tensile forces (Park JS *et al.* 2004, Maul TM *et al.* 2011). Additionally, specific shape geometries were engineered using adhesive micro-patterned surfaces (McBeath R *et al.* 2004, Kilian KA *et al.* 2010) and multi-perforated polycarbonate membranes (Yang Y *et al.* 1999). Thus, controlling MSC shape is an important method for investigating, understanding, and controlling MSC behavior *in vitro*.

The shape of individual cells is based on the balance between external biomechanical forces and internal cellular forces, and the level of internal forces is proportional to the elastic material properties of the surrounding extracellular matrix (Sun Y *et al.* 2012). Comprehensively this suggests that cell shape can be controlled through both matrix elasticity and biomechanical forces. We therefore hypothesized that specific MSC shapes can be generated as a function of the biomaterials chosen and the nanoscale stiffness associated with these biomaterials. Accordingly, we compared the shapes of human bone-marrow derived MSCs that adhered to different biomaterials with similar stiffnesses vs. similar biomaterial types with different stiffnesses, asking whether specific baseline shapes could be generated by altering biomaterial substrate properties. For this question, we used compressed collagen sheets as well as uncoated and fibronectin-coated silicone sheets. MSC shape was described using a semi-automated high-throughput method for calculating quantitative shape descriptors.

With cell shape being affected by the balance between external and internally generated forces, we theorized that changes in external force would prompt a subsequent change in shape. We hypothesized that the application of tensile forces results in MSC elongation *during* cyclic stretch, and that the effects on MSC elongation are diminished upon *cessation* of stretch. Hence, over time the MSC shape may revert towards its original biomaterial-dictated state much like an elastic rubber band released from tension. This was tested by comparing the shape of MSCs that adhered to cyclically stretched compressed collagen sheets to MSCs that adhered to non-stretched control sheets. Importantly, this setup established a system of two competing cues: dynamic effects on MSC shape through cyclic stretch and static effects on shape through the stiffness-defined biomaterial. This allowed us to answer whether dynamic cues on shape can potentially overpower static cues, or vice versa. Because elongated MSC morphologies are associated with increased expression of smooth muscle markers (Yang Y *et al.* 1999, Maul TM *et al.* 2011) and it has been shown that biomechanical forces can increase MSC differentiation towards a smooth muscle cell (SMC) phenotype (Hamilton DW *et al.* 2004, Nieponice A *et al.* 2007, Maul TM *et al.* 2011), we investigated how the generated MSC shapes correlated with MSC differentiation towards a SMC phenotype. The ability to understand and control MSC shape would be an important tool in directing the behavior of these cells and would advance the fields of biomaterials, biomechanics, and tissue engineering.

2 Materials and Methods

2.1 Biomaterials

2.1.1 Compressed collagen type I sheets

Compressed collagen was produced with Amedrix (Esslingen, Germany). Collagen type I fibers were isolated from de-skinned rat tails, washed in acetic acid for 24 h, purified, and lyophilized. Rat collagen type I hydrogels with an initial collagen concentration of 8 mg/ml were generated and mechanically compressed from initial thicknesses of 10 and 20 mm down to 1 mm thick sheets within a

custom-made polycarbonate chamber (20,0 x 2,7 x 5,0 cm) with a porous polytetrafluoroethylene (PTFE) bottom. The PTFE pore size was 100 µm to allow water effusion during compression. For hydrogel compression within the chamber, weights were used to generate compressed collagen with final concentrations of 80 and 160 mg/ml. 80 mg/ml sheets were generated with a weight of 2 kg applied for 2 hours, 4 kg applied overnight, 9,5 kg for 8 hours, and 27 kg overnight (total time of compression 34 hours). For 160 mg/ml sheets the final compression step applied 27 kg for 30 hours (total time of compression 52 hours).

2.1.2 Silicone sheets and silicone coating procedures

Non-reinforced vulcanized matt silicone sheets with thicknesses of 127 µm (termed thin) and 762 µm (termed thick) were obtained from Specialty Manufacturing (No. 70P001-200-005 and 70P001-200-030, both 40durometer-Shore-A, Saginaw, Michigan, USA). Thick silicone sheets were coated with fibronectin from bovine plasma (F1141, Sigma-Aldrich, Seinheim, Germany) diluted in PBS (12.5 µg/ml). Silicone sheets (2x1cm) were covered with 700 µl coating substrate in 12-well culture plates for 24h (room temperature), washed with 0.05 % Tween 20 in 2ml PBS, and washed 3x with 2ml PBS.

2.2 Atomic force microscopy (AFM)

AFM was performed to characterize the nanoscale stiffness of the biomaterial surfaces. Microspheres (Polybead Polystyrene 25.0 Micron Microspheres, Polysciences, Eppelheim, Germany) were attached to a tipless cantilever (All-in-One-cantilever D, 40 N/m nominal spring constant, Budget Sensors, Sofia, Bulgaria) using the M-Bond 610-1 adhesive single kit according to the manufacturer's instructions (Micro-Measurements, Vishay Precision Group, Wendell, USA). The cantilever of the atomic force microscope (CellHesion 200, JPK Instruments, Berlin, Germany) was calibrated on the extend curve and its spring constant was determined using the thermal noise method of the software (JPK Instruments).

Samples were measured with a maximum force of 800 nN and an extend speed of 5 µm/sec in triplicates at three locations for each sheet. The Young's modulus was calculated using the Hertz model fit of the data processing software (JPK Instruments).

2.3 Human bone marrow MSCs

2.3.1 Source

Bone-marrow samples were obtained with institutional approval of the local research ethics committee and with informed consent (reference number 623/2013BO2) from the proximal femur of patients undergoing total hip replacement (n=14, 50-86 years) in the Department of Trauma and Restorative Surgery, BG Trauma Clinic, University of Tuebingen.

2.3.2 Isolation, culture, and characterization

Bone marrow MSCs were prepared as described (Felka T *et al.* 2009). The samples were washed with PBS and centrifuged at 150 x g (10 min, room temperature) and resuspended with PBS. MSC were isolated using a Ficoll density gradient fractionation (density 1.077g/ ml, GE-Healthcare-Life-Sciences, Uppsala, Sweden, 400 x g, 30 min, room temperature). The mononuclear cell layer was harvested, washed with PBS and seeded in T75-flasks. MSC were expanded in good manufacturing practice (GMP)-compliant expansion medium consisting of DMEM low glucose (Sigma-Aldrich, Hamburg, Germany) including 25mM HEPES (2.4 % of total volume, Lonza Group, Basel, Switzerland), 0.2 % (1000IU) heparin (Carl Roth, Karlsruhe, Germany), 5 % human plasma (TCS Biosciences, Buckingham, UK), 5 % human pooled platelet lysate (10^8 platelets/ ml medium, UKT Tuebingen, Germany), 1 % L-glutamine (Lonza Group), and 1 % penicillin-streptomycin solution (Life Technologies, Darmstadt, Germany). After 24h (37°C, 5 % CO_2), medium was replaced to remove non-attached cells and GMP expansion medium was

changed twice a week. After 5-7 days, cells were removed with trypsin and re-seeded in GMP-expansion medium (passage 1, density $1.5x10^5$ cells/flask). The expression of MSC cell surface antigens and their adipogenic, osteogenic and chondrogenic differentiation were successfully demonstrated as we have shown previously (Felka T *et al.* 2009, Pilz GA *et al.* 2011, Ulrich C *et al.* 2013), and in accordance with (Dominici M *et al.* 2006) (data not shown).

2.4 MSCs on biomaterials

2.4.1 S*eeding and cell culture*

After expansion in GMP-expansion medium, MSCs were seeded at passages 2-5 (density: 5000 MSCs/cm^2) at day 0 onto the biomaterials and in medium consisting of DMEM high glucose (4 g/l, Life Technologies), 10 % FBS (Biochrom), 1 % penicillin-streptomycin solution (Life Technologies), and 1 % fungicide (Biochrom) at 37°C and 5 % CO_2**.** Upon binding of the MSCs to the different biomaterial surfaces used in this study, different cellular shapes appeared spontaneously. These were subject to further investigation.

2.4.2 *Sinusoidal cyclic stretch*

Compacted collagen sheets (80 mg/ ml) were seeded with MSCs at passages 2-5 at day 0 (n=13 bone marrow samples from n=8 donors, age range: 61-81 years, average age: 69.1 years, gender ratio: 1:1, seeding density: 5000 MSCs/cm^2). They were inserted at day 4 and day 5 into the bioreactor chamber (150 ml medium) of an incubator-housed ElectroForce-5210 BioDynamic-Test-System (Bose, Minnesota, USA), and stretched with displacement-controlled uniaxial cyclic stretch (strain: 2.5 and 5 % , 60 min, f=1 Hz) for 1h on day 4 and on day 5. Non-stretched MSCs served as controls. Each individual experiment consisted of 6 compacted collagen sheets: 2 controls, 2 sheets 1h after completion of 2.5 % stretch, and 2

sheets after 5 % stretch. The 1st sheet half was used for qRT-PCR, the 2nd half for fluorescence microscopy. To visualize MSCs during stretch, sheets were manually stretched on top of a microscope slide to a previously marked position (5 % stretch) and fixed to the slide with two clamps for fluorescence microscopy.

2.4.3 *Fluorescence microscopy*

The cellular shapes that were generated by the MSCs while attached to the various biomaterial surfaces were visualized by fluorescence microscopy. Cells were stained with the fluorescent dye calcein (Cell Viability Imaging Kit; Roche, Mannheim, Germany) according to the manufacturer's protocol to assess MSC shapes (see below). Adherent MSCs were digitally recorded in a top-down view (Zeiss LSM-510, AxioVison-4.8) according to (Rolauffs B *et al.* 2010, Rolauffs B *et al.* 2011). Image mosaics consisting of 10x10 tiles (12,633x9,429 pixel corresponding to 8,211.45x6,128.85 µm) were reconstructed (Module MosaiX) for cyclically stretched sheets and controls. For manually stretched sheets, mosaics of 17,629x7,564 pixel (11,458.85x4,916.6 µm) were reconstructed. The numbers of stained nuclei were counted using ImageJ (NIH, USA).

2.4.4 *MSC shape descriptors*

Calcein-stained MSCs were recorded using a Zeiss LSM-510 digital microscope and the images were processed to reconstruct image mosaics. Using ImageJ, the 4 shape descriptors roundness ($4*area/\pi*major\_axis\_length^2$), aspect ratio (major_axis_length/minor_axis_length), circularity ($4\pi*area/perimeter^2$), and solidity (area/convex_area) and the total number of cells/normalized area were calculated individually for each recorded cell. The user input was to set a manual threshold and the scale, which was 1.695 pixel per 1 µm. Then, a median filter with a radius of 2 pixel was applied for image smoothening prior to automated shape descriptor calculations.

2.4.5 *Gene expression (quantitative RT-PCR)*

Compressed collagen sheets were digested with Proteinase K (Fermentas/ThermoScientific, 4 min, 55°C). mRNA was isolated using the RNA-Extraction-RNeasy-Minikit (Qiagen, USA). cDNA was synthesized with the Advantage RT-for-PCR Kit (Clontech, USA). Quantitative RT-PCR was performed with the LightCycler-480 SybrGreen Master and LightCycler-480 Probes Master using a LightCycler 480 and 96-multiwell plates (Roche). Gene expression levels of alpha-smooth-muscle-actin (*ACTA2*), transgelin (*TAGLN*), calponin (*CNN1*), peptidylproplyl-isomerase-A (*PPIA*), and human glycerinaldehyde-3-phosphate-dehydrogenase (*GAPDH*) were determined according to MIQE guidelines (Bustin SA *et al.* 2009) (reference genes: *PPIA*, *GAPDH*). As positive controls and calibrator samples human bladder derived smooth muscle cells (HBdSMC, Promocell, Heidelberg, Germany) were used. The oligonucleotide primers were TTG CCT GAT GGG CAA GTG AT (forward primer sequence) and TAC ATA GTG GTG CCC CCT GA (reverse primer sequence) for *ACTA2*, AGA TGG CAT CAT TCT TTG CGA and GCT GGT GCC AAT TTT GGG TT for *CNN1*, CTC TGC TCC TCC TGT TCG and ACG ACC AAA TCC GTT GAC TC for *GAPDH*, and TTC ATC TGC ACT GCC AAG AC and TCG AGT TGT CCA CAG TCA GC for *PPIA*. For *TAGLN*, the Quiagen assay Hs_TAGLN_2_SG (QT01678516) was used. *For TAGLN* and *PPIA,* SybrGreen (Roche), and for *ACTA2*, *CNN1*, and *GAPDH* the Roche Universal Probe Library Probes N58 (*ACTA2*), N71 (*CNN1*), and N60 (*GAPDH*) were used. To confirm gene expression changes on protein level, Western blotting was performed (see supplementary material).

2.5 Statistical analyses

All data are presented as mean ± SEM except when box plots were chosen for data presentation. The box plots give the median, 25^{th} & 75^{th} as well as the 10^{th} & 90^{th} percentiles and outlying points. Calculations were performed with Microsoft Excel 2010 and SigmaPlot-11.0.0.77 (Systat, Chicago, USA). Data were analyzed for normality (Kolmogorov-Smirnov-test). For comparing two groups, normally distributed data were subjected to the Student's t-test and non-normal data were subjected to the Mann-

Whitney-Rank-Sum-Test. More than two groups were compared using ANOVA and appropriate post-hoc tests. Correlation analyses were performed using Spearman-Rank-Order-correlation-tests (non-normal data distribution) or Pearson-Product-Moment-correlation-tests (normal distribution). Differences were considered statistically significant (*) at $p<0.05$.

3 Results

3.1 Shape descriptors for quantifying MSC morphology

To illustrate the wide range of MSC shapes that we encountered throughout this study, Fig. 1A shows representative images of calcein-stained MSCs that were recorded digitally. Using these images, we quantitatively calculated the parameter roundness (see below, 3.2 shape descriptors) for each individual cell and sorted the depicted MSCs according to their corresponding roundness values. In addition, *in silico* patterns were drawn with Adobe Photoshop and Microsoft PowerPoint, and their shapes were calculated with the four quantitative shape descriptors roundness, aspect ratio, circularity, and solidity (see below) to demonstrate how these can be used to analyze MSC shape in detail, and how changes in shape can be quantified by these four shape descriptors (Fig. 1B,C). Panel D (Fig. 1D) is intended to be used by the reader as a reference chart to “translate” reported shape descriptor values into images.

3.2 Shape descriptors of MSCs adhering to various biomaterials

3.2.1 Shape descriptors of MSCs adhering to similar biomaterial types with different nanoscale stiffnesses

As a first step, we tested the effects of similar biomaterial types with different nanoscale stiffnesses on the four shape descriptors for MSCs that adhered to uncoated thick vs. thin silicone sheets (Fig. 2A-E). Interestingly, all shape descriptors were significantly different for MSCs on thick vs. thin silicone sheets ($p<0.001$, Fig. 2A-D). In particular, MSCs on thick silicone sheets exhibited a significantly

lower cellular roundness, higher aspect ratio and circularity, and a lower solidity, indicating a longer MSC morphology with smaller or less membrane protrusions, compared to MSCs on thin silicone sheets. To investigate a potential correlation with the nanoscale stiffness of the used biomaterials, we determined the nanoscale stiffness of the biomaterial surfaces by calculating the Young's modulus. For uncoated thick silicone sheets the Young's Modulus was 903.2±18.8 kPa. This value was significantly higher than the Young's Modulus of uncoated thin silicone sheets ($p<0.001$), which was 185.8±14.2 kPa (Fig. 2E). This suggested that higher nanoscale stiffness was associated with lower cellular roundness, higher aspect ratio and circularity, and a lower solidity.

3.2.2 Shape descriptors of MSCs adhering to different biomaterial types with similar nanoscale stiffnesses

We tested the effects of different biomaterial types with similar nanoscale stiffnesses on the four shape descriptors by comparing MSCs that adhered to uncoated vs. fibronectin-coated thick silicone sheets (Fig. 2F-J). There was no significant difference between the four shape descriptors of MSCs on uncoated vs. fibronectin-coated thick silicone sheets (Fig. 2F-I). To examine whether this could be explained by similar nanoscale stiffnesses of the two biomaterials, we determined their Young's Moduli. There was no significant difference in the nanoscale stiffness of the surfaces of uncoated (903.2±18.8 kPa) vs. fibronectin-coated (811.0±14.7 kPa) thick silicone sheets (Fig. 2J). This suggested that the MSC shape descriptor values were comparable on different materials with similar stiffnesses (uncoated and fibronectin-coated silicone), and that selected shape descriptor values were associated with the nanoscale stiffness of the biomaterials used for MSC adherence.

3.2.3 Shape descriptors of MSCs adhering to biomaterials with different collagen type I concentrations

We assessed the shape descriptors of MSCs that adhered to compacted collagen sheets produced with different collagen concentrations, and also the shape descriptors of MSCs on these compacted collagen sheets during day 4 and 5 (Fig. 2K-N). All shape descriptors of MSCs on compacted collagen type I sheets were significantly different, when comparing concentrations of 80 mg/ml vs. 160 mg/ml ($p<0.001$). In particular, MSCs on 80 mg/ml compacted collagen sheets exhibited a significantly lower roundness (Fig. 2K) and a higher aspect ratio (Fig. 2L), circularity (Fig. 2M) and solidity (Fig. 2N, $p<0.001$), indicating a longer MSC morphology with smaller or less membrane protrusions on 80 mg/ml sheets, compared to MSCs on 160 mg/ml sheets. When assessing the effect of time on 80 mg/ml and 160 mg/ml sheets (Fig. 2K-M), the shape descriptors roundness, aspect ratio, and circularity were not significantly different on day 4 vs. 5. In contrast, day 4 solidity was significantly higher than on day 5 ($p<0.001$, Fig. 2N), indicating that only MSC solidity but not the other shape descriptors underwent time-associated changes. Although differences in solidity were significant, they were relatively small. To correlate MSC shape descriptors with the nanoscale stiffness of the compacted collagen sheets, we calculated their Young's Modulus. The Young's Modulus of 80 mg/ml compacted collagen sheets was 10.2±0.8 kPa and significantly higher than the Young's Modulus of 160 mg/ml sheets ($p<0.001$), which was 7.2±0.6 kPa (Fig. 2O). As shown above for silicone sheets (Fig. 2A-E), these data indicated that lower roundness, higher aspect ratio and circularity, and a lower solidity were associated with a higher nanoscale stiffness of the same biomaterial type, presented here for compacted collagen sheets (Fig. 2K-O).

3.3 Effects of cyclic stretch on MSC shape descriptors

To assess the effects of tensile forces on MSC shape descriptors, we applied cyclic stretch to MSCs that adhered to compacted collagen sheets with a concentration of 80 mg/ml. This was also performed to assess whether the application of tensile forces results in MSC elongation during cyclic stretch, and whether the effects on elongation are diminished upon *cessation* of stretch. With both loading

regimes (2.5 % and 5 % strain amplitudes) and after a recovery period of 1h, cyclic stretch had significant effects on all four shape descriptors (Fig. 3A-D). The most obvious changes were that cyclic stretch significantly increased roundness (Fig. 3A), decreased aspect ratio (Fig. 3B), and increased circularity and solidity ($p<0.001$, Fig. 3C-D), when comparing non-stretched controls with cyclically stretched MSCs. Statistically, all differences between controls vs 2.5 % and controls vs 5 % stretched MSCs and between day 4 vs day 5 reached significant levels for all 4 shape descriptors ($p<0.001$). Assessing the effects of time on non-stretched and cyclically stretched MSCs, all four shape descriptors were significantly different ($p<0.001$, Fig. 3A-D). The stretch-induced increase in roundness on day 4 was diminished on day 5 (Fig. 3A) and the stretch-induced decrease in aspect ratio on day 4 was also diminished on day 5 (Fig. 3B). However, the stretch-induced increase in circularity was further increased (Fig. 3C) whereas stretch-induced responses in solidity depended on the strain amplitude (Fig. 3D). Thus, cyclic stretch had differential effects over time on roundness and aspect ratio vs. circularity. The non-stretched control MSCs also underwent significant changes in their cellular roundness, aspect ratio, circularity, and solidity when comparing days 4 and 5 ($p<0.001$). However, the changes observed over time in the non-stretched control MSCs were much smaller than the changes that were biomechanically induced. Collectively, these data demonstrated that biomechanical stretch of 2.5 % and 5 % was associated with a significant change in MSC morphology, and notably with a rounder MSC morphology (higher roundness, lower aspect ratio) with a smaller amount of membrane protrusions (higher circularity and solidity).

3.4 Changes in MSC shape descriptors after cessation of cyclic stretch

To demonstrate that stretching the biomaterial actually stretched the adhering cells, MSC-seeded compacted collagen sheets were manually stretched on top of a microscope slide, and the calcein-stained, unfixed MSCs were imaged (Fig. 4). Non-stretched control MSCs had an aspect ratio of 3.19 and a roundness of 0.398±0.002 (Fig. 4B,F). During cyclic stretch, the aspect ratio increased significantly to 3.34 ($p<0.001$) and roundness decreased significantly to 0.391±0.002 ($p<0.001$; Fig. 4 C,F). Thus, cyclic

stretch indeed increased aspect ratio (by 4.58 %) and decreased MSC roundness (by 1.82 %) consistent with the idea that elongated MSCs were produced during stretch ($p<0.001$). On day 4, 1h after the completion of cyclic stretch, the MSC roundness was significantly increased to 0.438±0.001 ($p<0.001$; Fig. 4D,F). Interestingly, this suggested that MSCs were rounder after cessation of stretch than during stretch. This was an unexpected observation, which indicated that biomechanically applied *elongation* of MSCs had led to *rounder* MSCs. Comparable findings were observed on day 5: 1h after the completion of cyclic stretch, the roundness was 0.425±0.001 and significantly higher than during stretch ($p<0.001$) but a little lower than on day 4 ($p<0.001$; Fig. E,F). Under the chosen conditions and with both amplitudes, cyclic stretch led to elongated MSCs *during* stretch but yielded rounder MSCs *after* the cessation of stretch; MSCs reverted back towards their original biomaterial-dictated shape. Collectively, this suggested that the effects of dynamically applied biomechanical forces overpowered the biomaterial-dictated static effects on shape, but only transiently.

3.5 Effects of cyclic stretch on MSC gene expression of SMC markers

To determine the effects of tensile forces on the gene expression of SMC markers, 2.5 % and 5 % cyclic stretch was applied to compacted collagen sheets (80 mg/ml) and the adhering MSCs. Those were subsequently analyzed by quantitative RT-PCR. Compared to non-stretched controls, 5 % cyclic stretch significantly increased the gene expression of *ACTA2* on day 5 (1.49±0.14-fold, $p<0.05$, Fig. 5A), the expression of *TAGLN* on day 5 (1.22±0.11, 1.71±0.14, $p<0.05$, Fig. 5B), and the expression of *CNN1* on day 4 (1.93±0.45, $p<0.05$, Fig. 5C). In contrast, 2.5 % cyclic stretch only significantly increased the expression of *TAGLN* on day 5. Thus, biomechanical stimulation via 5 % cyclic stretch for 1h for two consecutive days on (day 4 and day 5) induced the increased expression of the SMC marker genes *ACTA2*, *TAGLN*, and *CNN1*. These changes in the gene expression of SMC markers were confirmed on protein level (see supplementary material).

3.6 Biomechanical stimulation did not change MSC numbers

To assess whether biomechanical stimulation had any effects on proliferation, we calculated the total number of MSCs that adhered to compacted collagen sheets. However, the MSC numbers per normalized area did not significantly change when comparing day 4 and 5 controls, and when comparing cyclically stretched MSCs with controls, regardless of stretch duration or amplitude (see supplementary material). Thus, biomechanical stimulation had no effect on MSC numbers.

3.7 Correlations between biomechanically induced MSC shapes and SMC marker gene expression

Next, we performed a correlation analysis to determine if the biomechanically induced MSC shape descriptors correlated with the expression of specific SMC marker genes. The expression of *ACTA2* correlated significantly with roundness ($p<0.01$, correlation coefficient 0.309, Fig. 6A) and aspect ratio ($p<0.01$, -0.357, Fig. 6B). The expression of *TAGLN* correlated significantly with solidity ($p<0.05$, -0.223, Fig. 6C), and the expression of *CNN1* correlated significantly with roundness ($p<0.01$, 0.328, Fig. 6D), aspect ratio ($p<0.001$, -0.376, Fig. 6E), and circularity ($p<0.001$, 0.408, Fig. 6F). Increases in roundness and decreases in aspect ratio always correlated significantly with higher gene expression levels, and those were exclusively observed in the biomechanically stimulated MSCs. Increases in solidity and circularity correlated significantly with higher gene expression levels, which were only observed in the biomechanically stimulated MSCs. Correlations between *ACTA2* expression and circularity ($p=0.086$) or *TAGLN* expression and roundness ($p=0.064$) and aspect ratio ($p=0.051$) showed trends but did not significantly correlate. Thus, biomechanically-induced shape changes correlated significantly with changes in gene expression of specific SMC marker genes.

3.8 Relative shape descriptor changes as function of biomaterial type, concentration, application of cyclic stretch, and time

Table I presents absolute and relative values for the shape descriptors calculated. This allowed comparing the effects on MSC shape across the various experimental conditions. We used the color red

coding to illustrate relative decreases and green to illustrate relative increases. Biomaterial type, coating, concentration as well as culture time and the amplitude and loading time of cyclic stretch had all complex effects on MSC shape. However, the strength of the effects varied considerably.

4 Discussion

The present study demonstrates that both biomaterial and biomechanical cues determine MSC morphology measured via quantitative shape descriptors. First, we demonstrated that specific MSC baseline morphologies were associated with the nanoscale stiffness of the biomaterial surface to which the MSCs adhered. This is important because it implies that specific baseline shapes can be generated by choosing different biomaterial properties. Next, when applying cyclic tensional forces, we unraveled time- and amplitude-dependent effects on MSC shape and demonstrated that MSC elongation occurred *during* cyclic stretch, as was expected. Surprisingly though, *after cessation* of stretch MSC shape did not remain elongated; instead a significantly rounder cellular shape was observed. This suggested a remodeling effect of MSC shape in response to tensile forces which has not been previously described. Finally, we asked whether dynamic cues on cellular shape can potentially overpower static cues, or vice versa. To answer this question, we used a system of two competing cues with dynamic effects on MSC shape through cyclic stretch and static effects on shape through the stiffness-defined biomaterial. This approach demonstrated that the effects of dynamically applied biomechanical forces on cellular shape can overpower the biomaterial-dictated static effects on shape, but only transiently. Ultimately, MSC shape reverses back towards its original biomaterial-dictated state. The here generated insights broaden our methodology for measuring and understanding MSC shape under static and dynamic conditions. This will be helpful for designing the next generation of scaffolds aimed at directing MSC behavior under mechanical load *in situ*.

Since *ex vivo* MSC culturing performed on rigid tissue culture plastics may adversely affect the multipotency of MSCs (Zhang D and Kilian KA 2013), appropriate biomaterials with lineage-specific

biophysical cues may serve as a starting point to develop cell-based therapies, where endogenous *in vivo* signals can culminate to direct full differentiation (Lee J *et al.* 2014). Our first hypothesis was that specific MSC shapes can be generated as a function of the biomaterials chosen and the nanoscale stiffness associated with these biomaterials. We compared the shape of human bone-marrow derived MSCs that adhered to different biomaterials with similar stiffness (uncoated vs. fibronecin-coated silicone sheets), and also to similar biomaterial types with different stiffnesses (thin vs. thick silicone sheets, compacted collagen sheets with 80 mg/ml vs. 160 mg/ml collagen I concentration). Silicone sheets were previously used to investigate MSC behavior under cyclic stretch (Hamilton DW *et al.* 2004, Park JS *et al.* 2004, Liu B *et al.* 2008, Maul TM *et al.* 2011, Morita Y *et al.* 2013, Tondon A and Kaunas R 2014). Compacted collagen hydrogels compressed into dense sheets are termed compressed collagen (Brown RA *et al.* 2005) and were previously used for the tissue engineering of artificial corneas (Levis HJ *et al.* 2012) and skin (Braziulis E *et al.* 2012). We demonstrated here that higher nanoscale stiffness, compared to lower stiffness of the same biomaterial type, was associated with lower MSC roundness, higher aspect ratio and circularity, and a lower solidity. In strong contrast, similar nanoscale stiffnesses of different biomaterials were associated with statistically comparable MSC shape descriptors. These data strongly suggested that nanoscale stiffness has a significant effect on MSC shape descriptors. This implied that specific shapes can be generated by choosing specific nanoscale stiffnesses for MSC adherence. Other parameters such as fiber type and diameter of a given biomaterial also affect MSC morphology and specifically roundness (Phipps MC *et al.* 2011). Thus, when one would compare different biomaterial types with different nanoscale stiffnesses, a more complex situation would arise. This topic warrants attention through future studies. However, nanoscale stiffness is clearly a relevant biomaterial property for generating specific shapes of MSCs quantified with shape descriptors just as the present study demonstrates.

As demonstrated by this study shape descriptors can be used for describing MSC morphology in a quantitative fashion. In two recent publications, shape descriptors were successfully used for characterizing cellular shape in analyses pertaining to the differentiation of MSC into osteoblasts (Rocca A

et al. 2015) and to acute brain injury models in mice (Zanier ER *et al.* 2015). The descriptors roundness and aspect ratio are somewhat intuitive. A high roundness describes a rounder shape, whereas a high aspect ratio describes an elliptical shape (Fig. 1). These have shown to be relevant factors as rounded MSC shapes can aid adipogenic differentiation, while elongated shapes can aid myogenesis (Yang Y *et al.* 1999, Hamilton DW *et al.* 2004, Nieponice A *et al.* 2007, Maul TM *et al.* 2011) and osteogenic differentiation (McBeath R *et al.* 2004). Circularity and solidity can be understood best in terms of membrane protrusions such as lamellipodia (broad, flat protrusions at the leading edge of cells), filopodia (finger-like protrusions), and blebs (outward bulges in the plasma membrane) that are relevant for adhesion, migration, and rigidity sensing (Krause M and Gautreau A 2014). High values for circularity and solidity indicate fewer of such protrusions. Specifically, it appears that circularity may be a better indication of filopodia presence as it would drop significantly as the number of small protrusions rises. These small protuberances radically increase the perimeter which grows geometrically in the circularity measurement. Blebbing would have a less prominent effect on circularity but would greatly reduce solidity as the larger part of the cell is a concave area. These associations need to be confirmed in future studies. Our study demonstrated that the chosen methodology pertaining to shape analysis was successful in identifying differences in MSC shape across the experimental conditions tested. This was, in part, due to the semi-automated approach and a large number of data points (cells analyzed) that were acquired (44444 to 60594 MSCs) per condition. Another question raised by our data pertains to the apparently relatively small amount(s) of the induced changes in MSC morphology. E. g. 5 % stretch led to a maximum change of 10 % roundness and 7 % aspect ratio, whereas biomaterial-associated changes in shape induced a change of 20 % roundness and 34 % aspect ratio. To demonstrate the relevance of these relatively small amounts in the context of the literature, we analyzed geometrically defined micro-engineered adhesion sites used in (Kilian KA *et al.* 2010). This study used rounded pentagonal geometries for inducing adipogenic and edged pentagonal geometries for inducing osteogenic differentiation of MSCs. We calculated a difference of 3 % roundness and also 3 % aspect ratio between the two shape types, illustrating together with the

present study that small changes in MSC morphology can have a large impact.

Next, we focused on cyclic stretch-induced changes in MSC shape. The underlying hypothesis was that tensile forces may result in MSC elongation during cyclic stretch, but this is relieved upon cessation of stretch, as a consequence of diminished external force input. *In vivo*, the mechanical environment surrounding the stem cells changes dynamically (Sun Y *et al.* 2012), and external biomechanical forces and matrix mechanics are key regulators of stem cell fate (Engler AJ *et al.* 2006, Sun Y *et al.* 2012). In this context, cyclic tensile forces have been successfully used for the stimulation of tenogenesis (Wang W *et al.* 2013), myogenesis (Maul TM *et al.* 2011), osteogenesis (Jagodzinski M *et al.* 2004), and chondrogenesis of the intervertebral disk (Driscoll TP *et al.* 2013) and articular cartilage (McMahon LA *et al.* 2008). Our data demonstrated that cyclic stretch of MSCs induced significant cell elongation during stretch that was comparable to the stretch applied to the underlying biomaterial which supports previous data (Maul TM *et al.* 2011). However, not much attention has been given to cell shapes *after* biomechanical stimulation. Usually, the experimental design of studies deploying cyclic stretch consisted of measuring cells immediately upon completion of stimulation (Hamilton DW *et al.* 2004, Park JS *et al.* 2004, Kurpinski K *et al.* 2006, Nieponice A *et al.* 2007, O'Cearbhaill ED *et al.* 2008, Zhang L *et al.* 2008, Ghazanfari S *et al.* 2009, Kurpinski K *et al.* 2009, Maul TM *et al.* 2011, Sarraf CE *et al.* 2011, Throm Quinlan AM *et al.* 2011) except for a live microscopy study (Tondon A and Kaunas R 2014) or studies that assessed the effects on MSC proliferation (Kurpinski K *et al.* 2006, Ghazanfari S *et al.* 2009). Moreover, few studies investigated MSC shape in combination with cyclic stretch (Zhang L *et al.* 2008, Ghazanfari S *et al.* 2009, Maul TM *et al.* 2011, Throm Quinlan AM *et al.* 2011). To our knowledge, the present study is the first to investigate MSC shape systematically before, during, and after the completion of cyclic stretch. Finally, we attempted to address whether dynamic cues or static cues had more influence over cell shape using a system of two competing cues with dynamic and static effects on MSC shape. Most surprisingly, we uncovered that cyclic stretch led over time to a rounder MSC shape. This clearly uncovered an unreported and novel idea of shape remodeling during the time period immediately following

biomechanical stimulation. This behavior is likely a consequence of diminished force input. It was not associated with proliferation-associated rounding since MSC numbers did not change significantly across the stretch experiment conditions, and because non-adherent MSC would be lost into the medium of the loading chamber. Thus, our data demonstrated that changes in MSC shape occurred during stretch but continued to occur after the completion of stretch, and that stretch had time-dependent effects on roundness and aspect ratio, and amplitude-dependent effects on roundness and circularity. Moreover, our data clearly demonstrated that biomaterial properties dictated MSC shape but this effect was temporarily overruled by cyclic biomechanical loading. Upon relieving cyclic biomechanical tension, MSC shape reverted back towards the shape associated with the biomaterial. Moreover, the reversal of shape from the stretch-generated values towards the biomaterial-associated shape values caused the shapes to become even rounder, overshooting the initial roundness values seen prior to stretch. However, the roundness values were approximately similar to non-stretched controls after the second day of stretch. This implies that MSC shape generated during cyclic stretch could potentially be lost after stimulation is stopped, and that this occurs within a relatively short time. It also emphasizes that biomaterials could be designed to sustain or counteract biomechanically induced shapes. Thus, shape-controlling biomechanical forces and biomaterials could theoretically be used for differential or synergistic effects on MSC shape.

Given the range of MSC shapes generated here, we finally asked how the recorded shapes may relate to changes in gene expression. This was undertaken in the context of MSCs differentiating towards a SMC phenotype because dynamic elongation of MSCs is a well-recognized model for inducing a SMC phenotype (Hamilton DW *et al.* 2004, Nieponice A *et al.* 2007, Maul TM *et al.* 2011) and because elongated MSC morphologies are associated with increased expression of smooth muscle markers (Yang Y *et al.* 1999, Maul TM *et al.* 2011). A recent study uncovered that the attempt to drive differentiation of MSCs with soluble stimulators of smooth muscle differentiation was only successful when the MSCs were physically permitted to elongate (Yang Y *et al.* 1999). Thus, MSC elongation seemed relevant for inducing a SMC phenotype in MSCs. We reported in the previous section of the discussion that cyclic stretch led to

an elongated MSC shape but that cessation of stretch was associated with complex changes in MSC shape. The resulting shapes and the corresponding expression levels of myogenic marker genes are given in Fig. 6. Specific aspects of MSC morphology, quantified with cellular shape descriptors, correlated significantly with the expression levels of specific marker genes. In particular, *ACTA2* correlated with roundness and aspect ratio (Fig. 6A,B), *TAGLN* with solidity (Fig. 6C), and *CNN1* with roundness, aspect ratio, and circularity (Fig. 6D-F). Thus, shape and differentiation were clearly associated under the chosen conditions. Interestingly, lowest roundness, highest aspect ratio, and lowest circularity values were associated with lowest gene expression levels, occurring in the non-stretched controls. This is important because the nanoscale stiffness of the 80 mg/ml compacted collagen sheets was ~10 kPa and, thus, in the stiffness range of 8 to 17 kPa known to support myogenic differentiation of MSCs (Engler AJ *et al.* 2006). Nevertheless, the non-stretched control MSCs that experienced myogenic differentiation-supporting nanoscale stiffness through the compacted collagen sheets exhibited the lowest expression of SCM marker genes. In contrast, highest roundness, lowest aspect ratio, and highest circularity were associated with the highest expression of marker genes and were exclusively observed in the biomechanically stretched groups. This biomechanically induced increase in SMC marker expression was confirmed on protein level (see supplementary material). One interpretation is that the added effects of tensional force and biomaterial stiffness were more effective in inducing the gene expression of SMC markers in MSCs than stiffness alone. This is supported by (Kurpinski K *et al.* 2009) who demonstrated that a synergistic upregulation of *CNN1* through TGF-β1 in combination with cyclic stretch was greater than the increase in response to either stimulus alone. Additionally, our data emphasized that specific shape descriptor values were associated (and significantly correlated) with specific marker profiles. For example, a roundness value of approximately 0.4 and an aspect ratio value of 3.4 were critical values for the highest gene expression levels of *ACTA2* and *CNN1*, observed under the chosen conditions. Circularity values higher than 0.35 were critical for a high expression of *CNN1*. Thus, specific shape descriptor values may serve as a future template for the induction of SMC phenotype and may be adapted

for other differentiation lineages as well. Finally, these data illustrate that even subtle differences in MSC morphology may provide a relevant impact on MSC behavior, and that using quantitative shape descriptors is a suitable method for studying this impact.

5 Conclusion

The present study demonstrates that MSC morphology can be measured using quantitative shape descriptors. MSC shape was surprisingly dynamic and could be manipulated through different methods. Dynamic tensile forces were more effective in defining MSC shape than stiffness-related cues. However, the biomechanical effects on cellular shape were transient and MSC shape ultimately reversed back to the shape dictated by biomaterial properties. A potential application of this insight would be to develop shape-instructive biomaterials, which transduce the dynamic *in vivo* biomechanical environment into specific MSC shapes for controlling MSC behavior.

6 Acknowledgements

We are very grateful for the support which we received from the German Research Council (RO2511/3-1 to B.R.; KL709/13-1 to G.K.; AI16/23-1 to W.K.A.), the German Ministry of Education and Research (BMBF) and the company AESCULAP (01KQ0902B REGiNA TP2 (BR)), which supported acquisition of the Bose ElectroForce 5210 BioDynamic-Test-System, and the intramural financial and personnel support of the BG Trauma Clinic Tuebingen (Berufsgenossenschaftliche Unfallklinik Tuebingen) and the clinic operator Heidelberg Association for the Treatment of Occupational Injuries (Verein für Berufsgenossenschaftliche Heilbehandlung Heidelberg e.V.).

7 Figure Captions

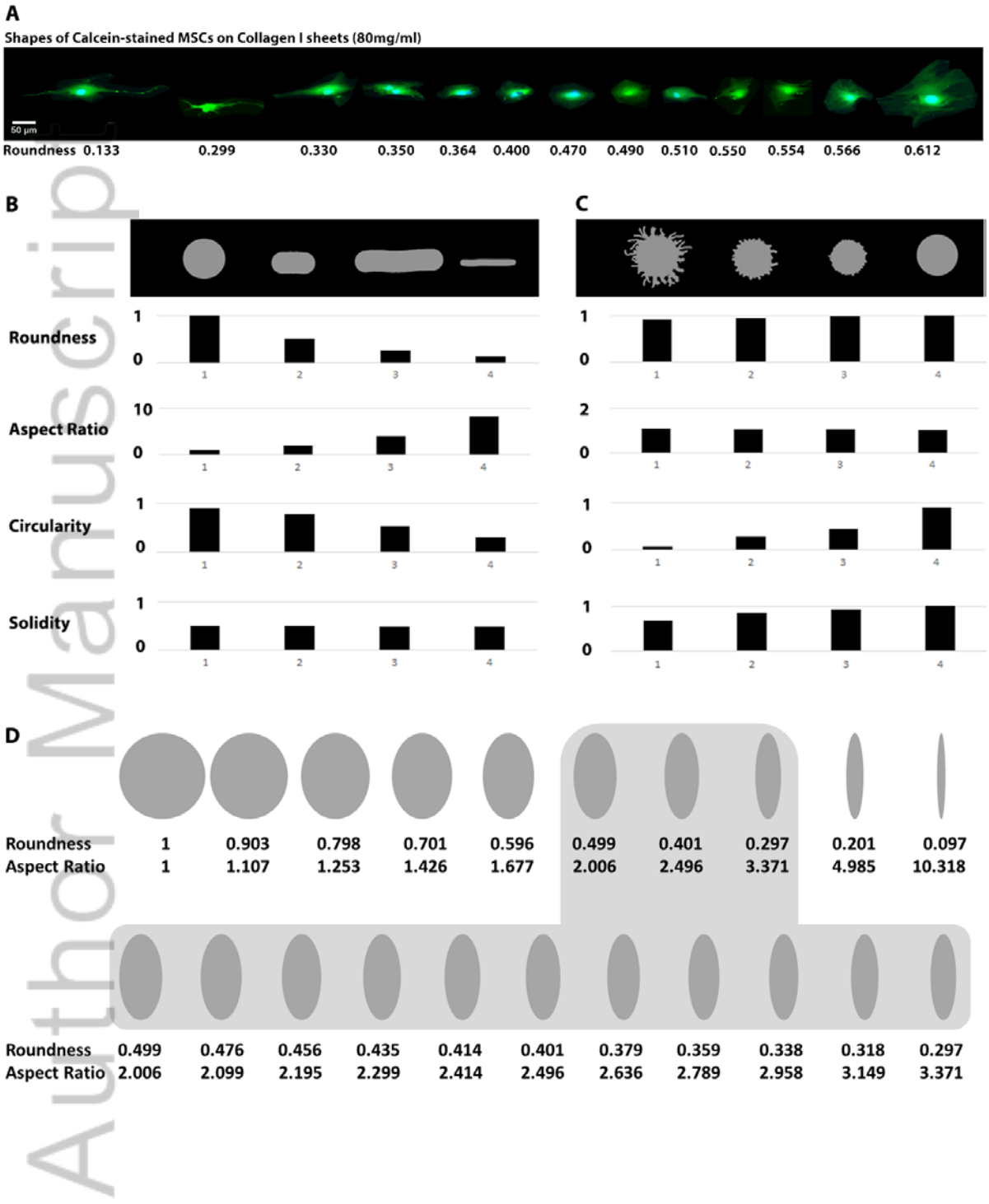

Figure 1. ***Range of observed MSC shapes and shapes drawn in silico to illustrate how changes in shape can be quantified by shape descriptors*****.** Human MSCs that adhered to the surfaces of compacted collagen type I sheets were stained with the fluorescent dye calcein and recorded in a top-down view. The shape descriptor "roundness" was calculated for each cell individually. (A) Representative images depicting individual MSCs and their associated roundness are given to illustrate the broad range of shapes that was observed in this study. Scale bar, 50 µm. (B) Panel B illustrates how a circular shape morphing into an elongated shape is best quantified with the descriptors roundness and aspect ratio. A high value for roundness indicates a round cell, and a high aspect ratio indicates a rather elongated cell. High values for both circularity and solidity indicate the absence of (cellular) protrusions. (C) Panel C illustrates how a circle with a large amount of protrusions morphing into a circle without protrusions is best quantified by the descriptors circularity and solidity, while roundness and aspect ratio remain unchanged. (D) Panel D is intended as a reference chart to "translate" reported shape descriptor values into images by providing standardized shape changes, analogous to commonly used standard curves.

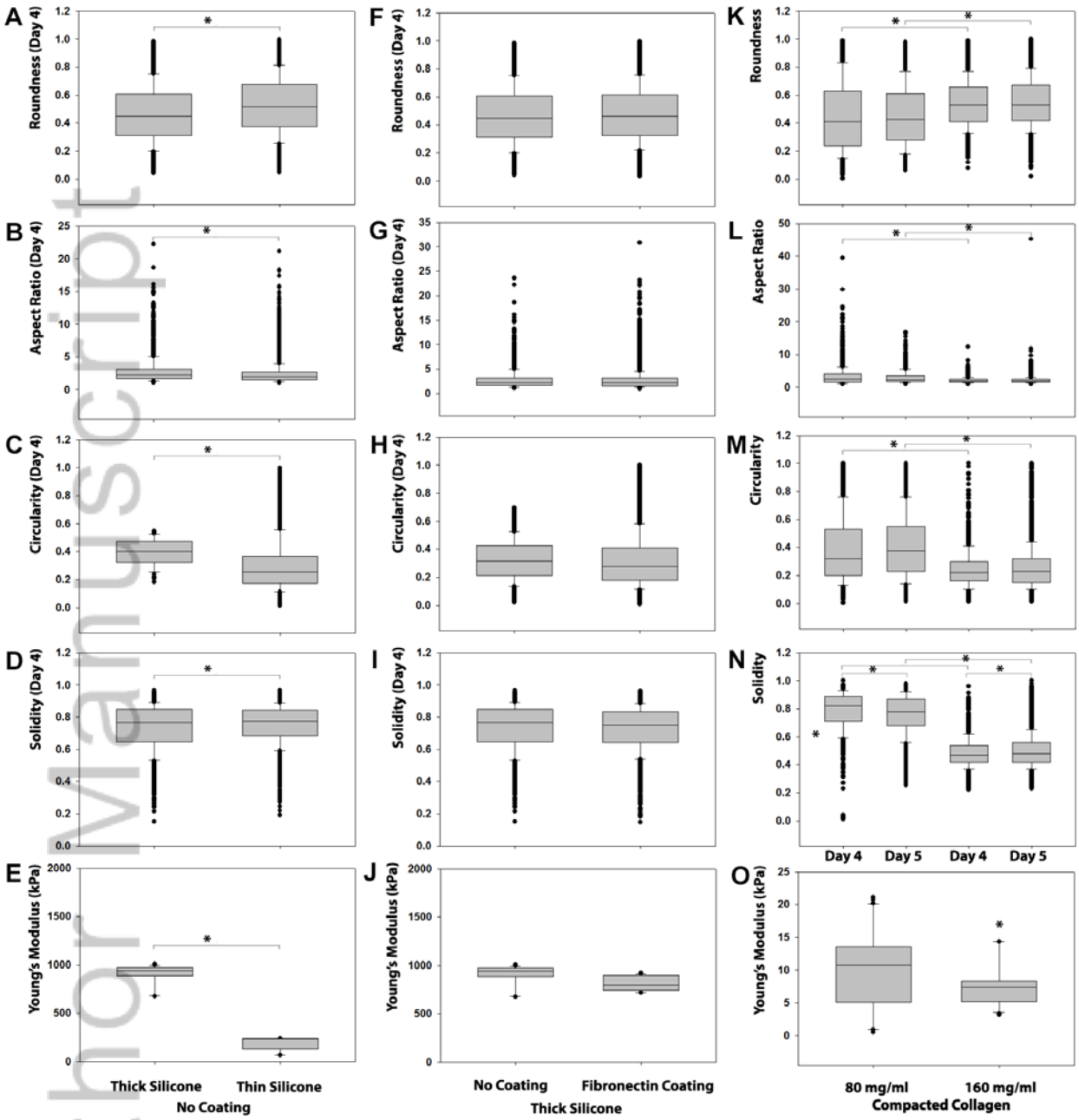

Figure 2. ***MSC shape descriptors and nanoscale surface stiffness of thick and thin silicone sheets, thick silicone sheets coated with fibronectin, and 80 and 160 mg/ml compacted collagen sheets.*** This figure reports the shape descriptors roundness (A,F,K), aspect ratio (B,G,L), circularity (C,H,M), and solidity (D,I,N) of calcein-stained MSCs that adhered to the selected biomaterial surfaces (thick/thin silicone: A-D; thick uncoated /fibronectin-coated silicone: F-I; 80 and 160 mg/ml compacted collagen type I on days 4 and 5: K-N), as well as the nanoscale stiffness of these surfaces measured with AFM (E, J, O). The figure illustrates significant differences in all four shape descriptors of MSCs adhering to thick vs thin silicone sheets ($p<0.001$, A-D), and also differences in the nanoscale stiffness of the thick vs. thin silicone sheets ($p<0.001$, E). In strong contrast, the four shape descriptors were not significantly different when comparing thick uncoated silicone sheets vs. thick fibronectin-coated silicone sheets (F-I). Additionally, there was no significant difference in the nanoscale stiffness between the uncoated and fibronectin-coated silicone surfaces (J). There were significant differences in the shape descriptors of MSCs adhering to 80 mg/ml vs. 160 mg/ml compacted collagen sheets ($p<0.001$, K-N) and small but significant differences in the nanoscale stiffness between these sheets (O). The box plots give the median and the 25^{th} & 75^{th} percentiles, the error bars give the 10^{th} & 90^{th} percentiles, and outliers are presented in light grey. ***** indicate significant differences with $p<0.05$. Number of individually performed experiments for calculating shape descriptors: n=3 sheets for each condition, n=2675 - 9056 MSCs per condition (silicone) and n=1290 - 6209 MSCs per condition (compacted collagen). Number of individually performed experiments for AFM: n=3 sheets for each biomaterial category, n=9 different measurement points per sheet.

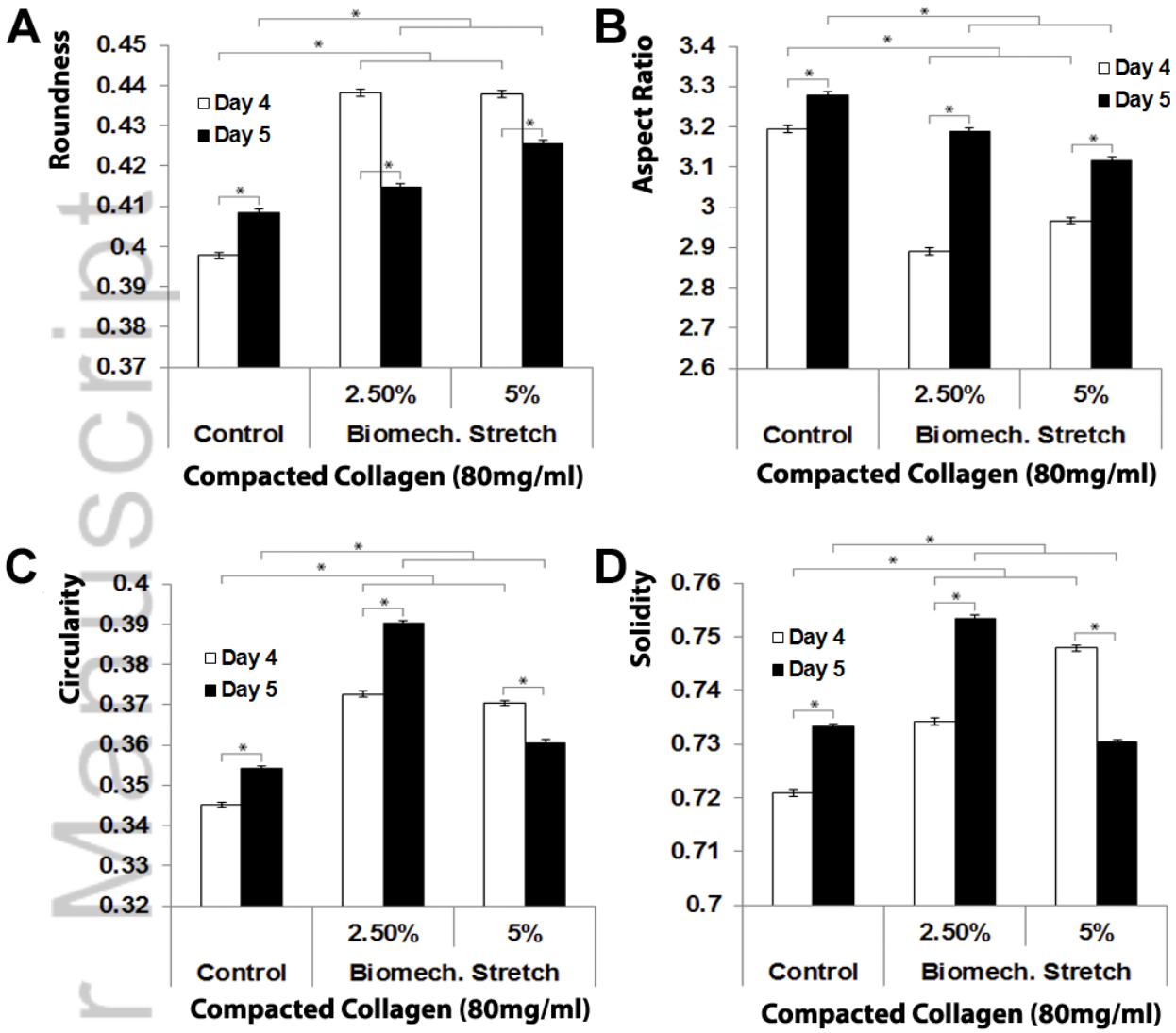

Figure 3. ***Shape descriptors of MSCs adhering to cyclically stretched 80 mg/ml compacted collagen sheets.*** This figure illustrates significant differences in the shape descriptors roundness (A), aspect ratio (B), circularity (C), and solidity (D) when comparing cyclically stretched vs. non-stretched control MSCs ($p<0.001$). The box plots give the median and the 25^{th} & 75^{th} percentiles, the error bars give the 10^{th} & 90^{th} percentiles, and outliers are presented in light grey. ***** indicate significant differences with $p<0.05$. Number of individually performed experiments for cyclic stretch: n=13 sheets for each loading regime, n=44444 - 60594 MSCs for each loading regime.

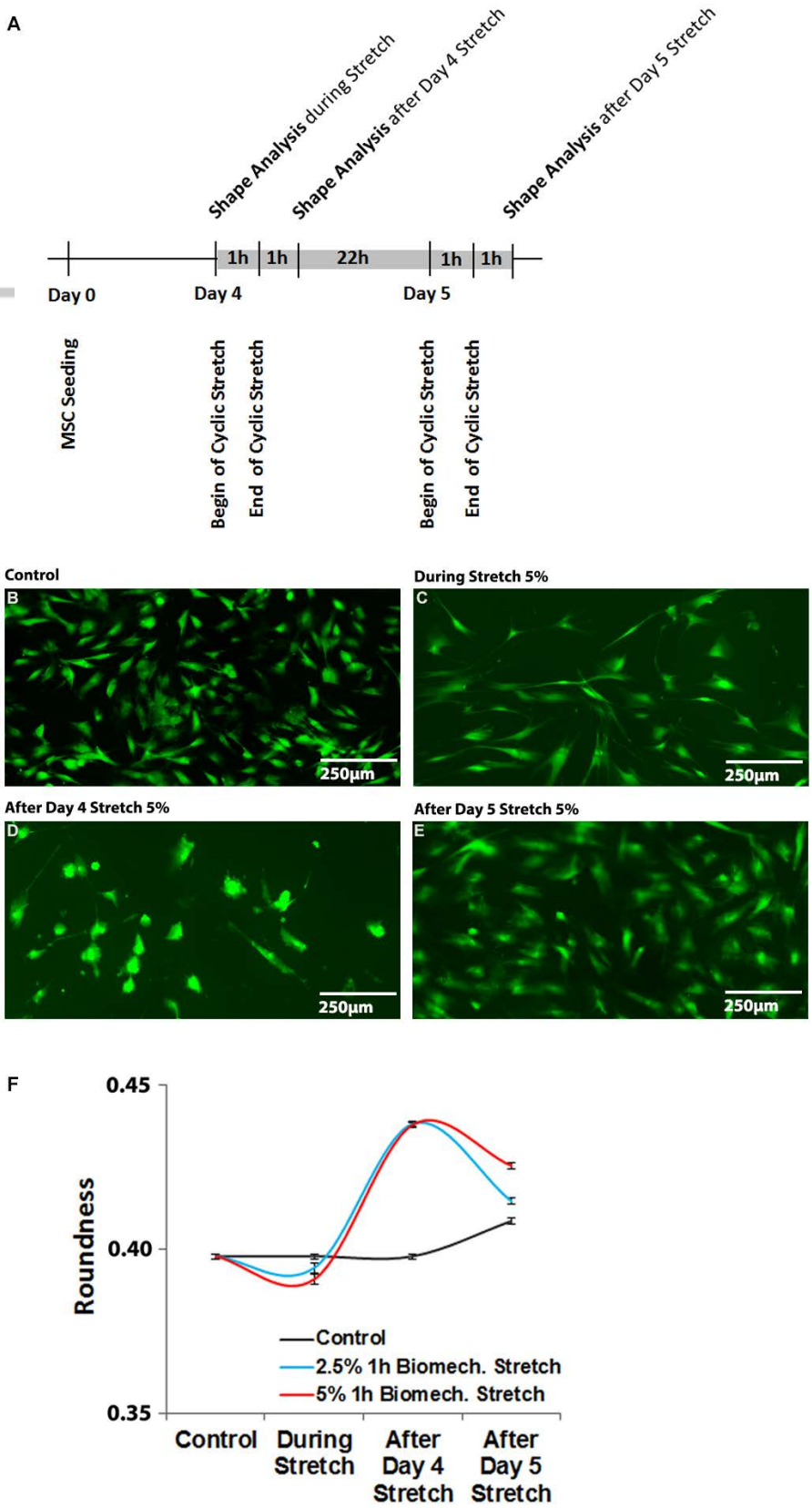

Figure 4. ***Experimental timeline and changes in MSC shape descriptors after cessation of cyclic stretch.*** (A) The experimental timeline for cyclic stretch and subsequent analyses. Using representative images of calcein-stained MSCs in a top-down view onto the surface of compacted collagen type I sheets, this figure illustrates the roundness values of non-stretched control MSCs (B), of MSCs during static stretch (C), 1h after cessation of 5 % cyclic stretch on day 4 (D), and 1h after cessation of 5 % cyclic stretch on day 5 (E). (F) Average roundness and standard errors at these time points (5 % stretch amplitude: red line, 2.5 % amplitude: blue line). Data in F is presented as mean±SEM. Number of individually performed experiments: n=13 for controls and n=14 for days 4 and 5 cyclic stretch; n=5 for values recorded during stretch.

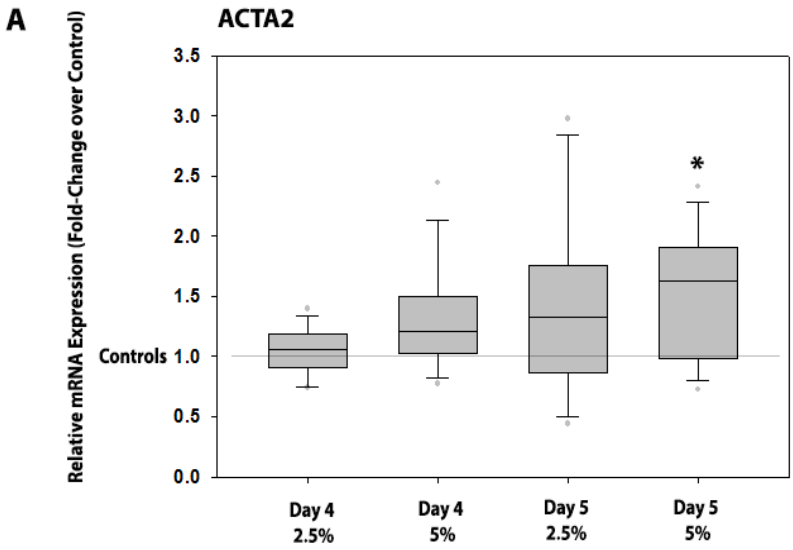

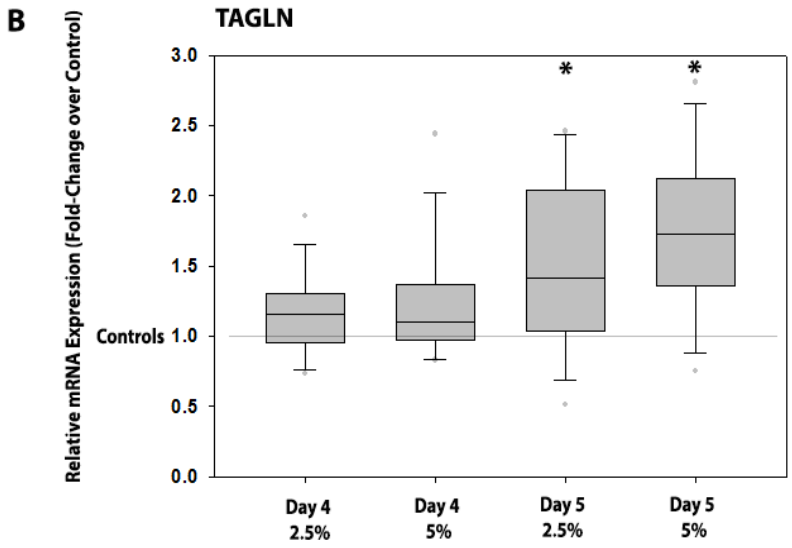

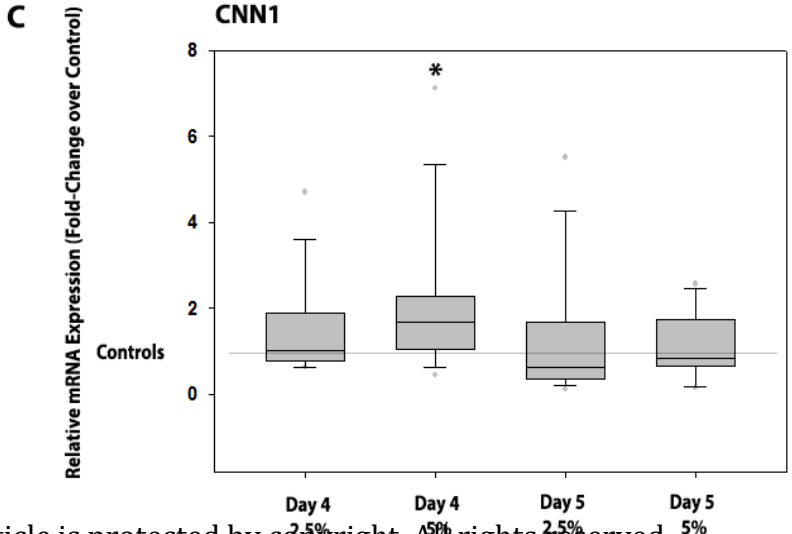

Figure 5. ***Biomechanically induced changes in gene expression of SMC markers.*** This figure reports the gene expression levels (relative mRNA expression) of *ACTA2 (A)*, *TAGLN (B)*, and *CNN1* (C) of cyclically stretched MSCs, normalized to unstimulated control MSCs (data is presented in fold-change; a value = 1 represents the gene expression level of unstimulated controls for day 4 and 5). Cyclic stretch was performed with 2.5 % and strain 5 % amplitude for 1h per day on days 4 and 5 at a frequency of 1Hz. 80 mg/ml compacted collagen sheets were stretched together with the adhering MSCs, seeded at a density of 5000 MSCs per cm^2. The box plots give the median and the 25^{th} & 75^{th} percentiles, the error bars give the 10^{th} & 90^{th} percentiles, and outliers are presented in light grey. ***** indicate significant differences with $p<0.05$. Number of individually performed experiments: n=13 for each condition.

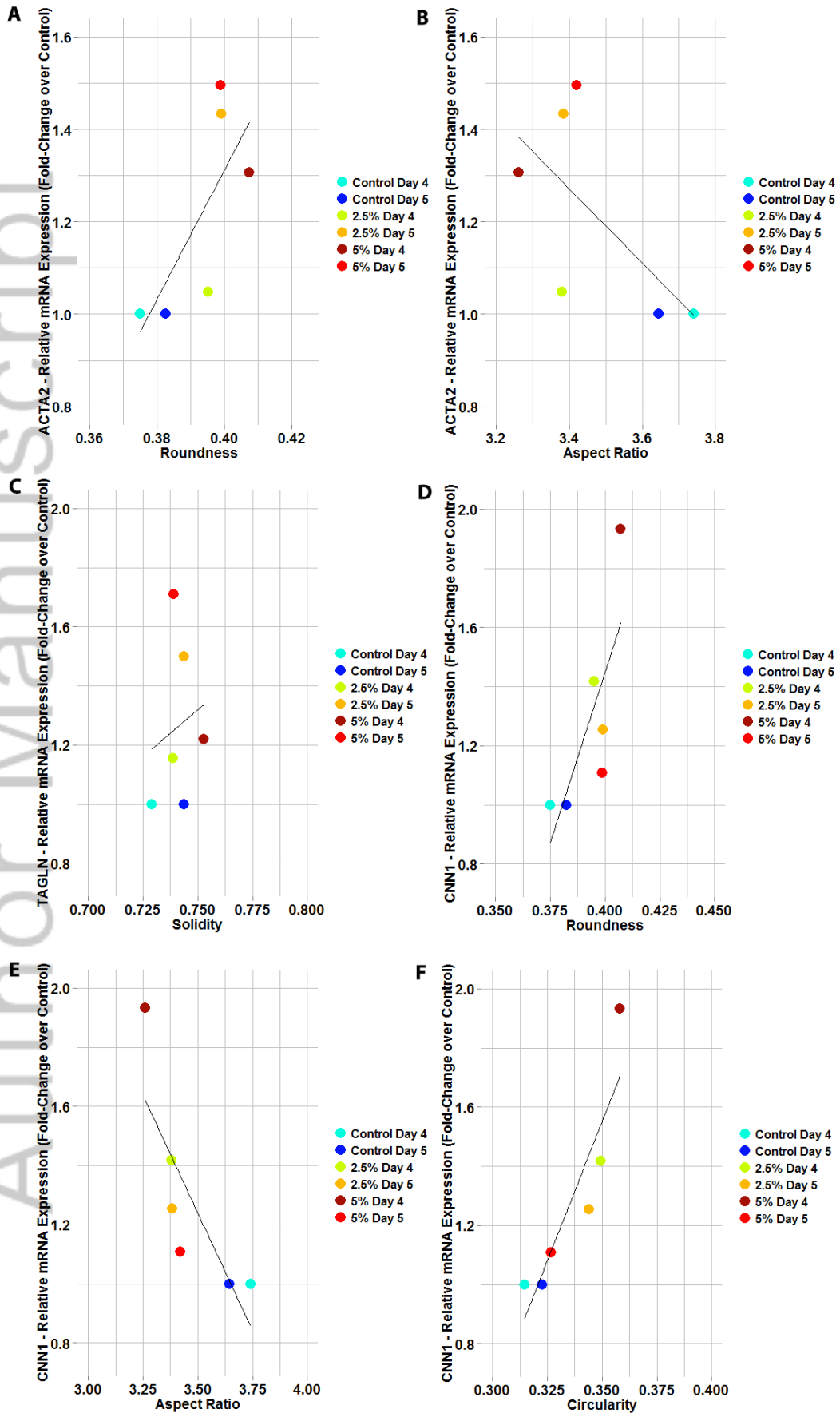

Figure 6. ***Correlations between biomechanically induced changes in MSC shape descriptors and gene expression levels of SMC markers.*** On the x-axis, this figure reports the shape descriptor values of MSCs for unstimulated controls and 2.5 % and 5 % cyclically stretched MSCs. On the y-axis, this figure reports the gene expression levels of *ACTA2 (A,B)*, *TAGLN (C)*, and *CNN1* (D-F) of biomechanically stimulated MSCs normalized to unstimulated controls (controls=1). Only correlations between shape descriptors and gene expression levels that reached significant levels are presented. Each panel also gives the calculated linear regression line between MSC morphology and gene expression. A single data point represents the average of n=13 individual experiments on the x-axis. For each individual experiment, all four shape descriptors were calculated for each individual cell that was recorded (day 4 control: n=60385 MSCs, day 4 2.5 % stretch: n=50721 MSCs, day 4 5 % stretch: n= 60329 MSCs, day 5 control: n=60594 MCSs, day 5 2.5 % stretch: n=44444 MSCs, day 5 5 % stretch: n= 49623 MSCs). On the y-axis, a single data point represents the average mRNA expression of all adherent MSCs, assessed by qRT-PCR for each individual experiment (n=13).

9 References

Aicher, WK, Buhring HJ, Hart M, Rolauffs B, Badke A, Klein G (2011). "Regeneration of cartilage and bone by defined subsets of mesenchymal stromal cells--potential and pitfalls." *Advanced drug delivery reviews* **63**(4-5): 342-351.

Braziulis, E, Diezi M, Biedermann T, Pontiggia L, Schmucki M, Hartmann-Fritsch F, Luginbuhl J, Schiestl C, Meuli M, Reichmann E (2012). "Modified plastic compression of collagen hydrogels provides an ideal matrix for clinically applicable skin substitutes." *Tissue engineering. Part C, Methods* **18**(6): 464-474.

Brown, RA, Wiseman M, Chuo CB, Cheema U, Nazhat SN (2005). "Ultrarapid Engineering of Biomimetic Materials and Tissues: Fabrication of Nano- and Microstructures by Plastic Compression." *Adv Funct Mater* **15**(11): 1762-1770.

Bustin, SA, Benes V, Garson JA, Hellemans J, Huggett J, Kubista M, Mueller R, Nolan T, Pfaffl MW, Shipley GL, Vandesompele J, Wittwer CT (2009). "The MIQE guidelines: minimum information for publication of quantitative real-time PCR experiments." *Clinical chemistry* **55**(4): 611-622.

Caplan, AI (2007). "Adult mesenchymal stem cells for tissue engineering versus regenerative medicine." *J Cell Physiol* **213**(2): 341-347.

Dominici, M, Le Blanc K, Mueller I, Slaper-Cortenbach I, Marini F, Krause D, Deans R, Keating A, Prockop D, Horwitz E (2006). "Minimal criteria for defining multipotent mesenchymal stromal cells. The International Society for Cellular Therapy position statement." *Cytotherapy* **8**(4): 315-317.

Driscoll, TP, Nakasone RH, Szczesny SE, Elliott DM, Mauck RL (2013). "Biaxial mechanics and inter-lamellar shearing of stem-cell seeded electrospun angle-ply laminates for annulus fibrosus tissue engineering." *J Orthop Res* **31**(6): 864-870.

Engler, AJ, Sen S, Sweeney HL, Discher DE (2006). "Matrix elasticity directs stem cell lineage specification." *Cell* **126**(4): 677-689.

Felka, T, Schafer R, Schewe B, Benz K, Aicher WK (2009). "Hypoxia reduces the inhibitory effect of IL-1beta on chondrogenic differentiation of FCS-free expanded MSC." *Osteoarthritis Cartilage* **17**(10): 1368-1376.

Folkman, J, Moscona A (1978). "Role of cell shape in growth control." *Nature* **273**(5661): 345-349.

Ghazanfari, S, Tafazzoli-Shadpour M, Shokrgozar MA (2009). "Effects of cyclic stretch on proliferation of mesenchymal stem cells and their differentiation to smooth muscle cells." *Biochem Biophys Res Commun* **388**(3): 601-605.

Hamilton, DW, Maul TM, Vorp DA (2004). "Characterization of the response of bone marrow-derived progenitor cells to cyclic strain: implications for vascular tissue-engineering applications." *Tissue Eng* **10**(3-4): 361-369.

Jagodzinski, M, Drescher M, Zeichen J, Hankemeier S, Krettek C, Bosch U, van Griensven M (2004). "Effects of cyclic longitudinal mechanical strain and dexamethasone on osteogenic

differentiation of human bone marrow stromal cells." *European cells & materials* **7**: 35-41; discussion 41.
Kilian, KA, Bugarija B, Lahn BT, Mrksich M (2010). "Geometric cues for directing the differentiation of mesenchymal stem cells." *Proc Natl Acad Sci U S A* **107**(11): 4872-4877.
Klein, G, Hart ML, Brinchmann JE, Rolauffs B, Stenzl A, Sievert KD, Aicher WK (2015). "Mesenchymal stromal cells for sphincter regeneration." *Advanced drug delivery reviews* **82-83**: 123-136.
Krause, M, Gautreau A (2014). "Steering cell migration: lamellipodium dynamics and the regulation of directional persistence." *Nature reviews. Molecular cell biology* **15**(9): 577-590.
Kurpinski, K, Chu J, Hashi C, Li S (2006). "Anisotropic mechanosensing by mesenchymal stem cells." *Proc Natl Acad Sci U S A* **103**(44): 16095-16100.
Kurpinski, K, Chu J, Wang D, Li S (2009). "Proteomic Profiling of Mesenchymal Stem Cell Responses to Mechanical Strain and TGF-beta1." *Cell Mol Bioeng* **2**(4): 606-614.
Lee, J, Abdeen AA, Kilian KA (2014). "Rewiring mesenchymal stem cell lineage specification by switching the biophysical microenvironment." *Scientific reports* **4**: 5188.
Levis, HJ, Peh GS, Toh KP, Poh R, Shortt AJ, Drake RA, Mehta JS, Daniels JT (2012). "Plastic compressed collagen as a novel carrier for expanded human corneal endothelial cells for transplantation." *PloS one* **7**(11): e50993.
Liu, B, Qu MJ, Qin KR, Li H, Li ZK, Shen BR, Jiang ZL (2008). "Role of cyclic strain frequency in regulating the alignment of vascular smooth muscle cells in vitro." *Biophys J* **94**(4): 1497-1507.
Manasek, FJ, Burnside MB, Waterman RE (1972). "Myocardial cell shape change as a mechanism of embryonic heart looping." *Dev Biol* **29**(4): 349-371.
Maul, TM, Chew DW, Nieponice A, Vorp DA (2011). "Mechanical stimuli differentially control stem cell behavior: morphology, proliferation, and differentiation." *Biomech Model Mechanobiol* **10**(6): 939-953.
McBeath, R, Pirone DM, Nelson CM, Bhadriraju K, Chen CS (2004). "Cell shape, cytoskeletal tension, and RhoA regulate stem cell lineage commitment." *Developmental cell* **6**(4): 483-495.
McMahon, LA, Reid AJ, Campbell VA, Prendergast PJ (2008). "Regulatory effects of mechanical strain on the chondrogenic differentiation of MSCs in a collagen-GAG scaffold: experimental and computational analysis." *Ann Biomed Eng* **36**(2): 185-194.
Morita, Y, Watanabe S, Ju Y, Xu B (2013). "Determination of optimal cyclic uniaxial stretches for stem cell-to-tenocyte differentiation under a wide range of mechanical stretch conditions by evaluating gene expression and protein synthesis levels." *Acta of bioengineering and biomechanics / Wroclaw University of Technology* **15**(3): 71-79.
Nieponice, A, Maul TM, Cumer JM, Soletti L, Vorp DA (2007). "Mechanical stimulation induces morphological and phenotypic changes in bone marrow-derived progenitor cells within a three-dimensional fibrin matrix." *J Biomed Mater Res A* **81**(3): 523-530.
O'Cearbhaill, ED, Punchard MA, Murphy M, Barry FP, McHugh PE, Barron V (2008). "Response of mesenchymal stem cells to the biomechanical environment of the endothelium on a flexible tubular silicone substrate." *Biomaterials* **29**(11): 1610-1619.

Park, JS, Chu JS, Cheng C, Chen F, Chen D, Li S (2004). "Differential effects of equiaxial and uniaxial strain on mesenchymal stem cells." *Biotechnology and bioengineering* **88**(3): 359-368.
Phipps, MC, Clem WC, Catledge SA, Xu Y, Hennessy KM, Thomas V, Jablonsky MJ, Chowdhury S, Stanishevsky AV, Vohra YK, Bellis SL (2011). "Mesenchymal stem cell responses to bone-mimetic electrospun matrices composed of polycaprolactone, collagen I and nanoparticulate hydroxyapatite." *PloS one* **6**(2): e16813.
Pilz, GA, Ulrich C, Ruh M, Abele H, Schafer R, Kluba T, Buhring HJ, Rolauffs B, Aicher WK (2011). "Human term placenta-derived mesenchymal stromal cells are less prone to osteogenic differentiation than bone marrow-derived mesenchymal stromal cells." *Stem Cells Dev* **20**(4): 635-646.
Rocca, A, Marino A, Rocca V, Moscato S, de Vito G, Piazza V, Mazzolai B, Mattoli V, Ngo-Anh TJ, Ciofani G (2015). "Barium titanate nanoparticles and hypergravity stimulation improve differentiation of mesenchymal stem cells into osteoblasts." *International journal of nanomedicine* **10**: 433-445.
Rolauffs, B, Rothdiener M, Bahrs C, Badke A, Weise K, Kuettner KE, Kurz B, Aurich M, Grodzinsky AJ, Aicher WK (2011). "Onset of preclinical osteoarthritis: the angular spatial organization permits early diagnosis." *Arthritis Rheum* **63**(6): 1637-1647.
Rolauffs, B, Williams JM, Aurich M, Grodzinsky AJ, Kuettner KE, Cole AA (2010). "Proliferative remodeling of the spatial organization of human superficial chondrocytes distant from focal early osteoarthritis." *Arthritis Rheum* **62**(2): 489-498.
Sarraf, CE, Otto WR, Eastwood M (2011). "In vitro mesenchymal stem cell differentiation after mechanical stimulation." *Cell proliferation* **44**(1): 99-108.
Singhvi, R, Kumar A, Lopez GP, Stephanopoulos GN, Wang DI, Whitesides GM, Ingber DE (1994). "Engineering cell shape and function." *Science* **264**(5159): 696-698.
Sun, Y, Chen CS, Fu J (2012). "Forcing stem cells to behave: a biophysical perspective of the cellular microenvironment." *Annual review of biophysics* **41**: 519-542.
Throm Quinlan, AM, Sierad LN, Capulli AK, Firstenberg LE, Billiar KL (2011). "Combining dynamic stretch and tunable stiffness to probe cell mechanobiology in vitro." *PloS one* **6**(8): e23272.
Tondon, A, Kaunas R (2014). "The direction of stretch-induced cell and stress fiber orientation depends on collagen matrix stress." *PloS one* **9**(2): e89592.
Ulrich, C, Rolauffs B, Abele H, Bonin M, Nieselt K, Hart ML, Aicher WK (2013). "Low osteogenic differentiation potential of placenta-derived mesenchymal stromal cells correlates with low expression of the transcription factors Runx2 and Twist2." *Stem Cells Dev* **22**(21): 2859-2872.
Wang, W, Deng D, Li J, Liu W (2013). "Elongated cell morphology and uniaxial mechanical stretch contribute to physical attributes of niche environment for MSC tenogenic differentiation." *Cell biology international* **37**(7): 755-760.
Yang, Y, Relan NK, Przywara DA, Schuger L (1999). "Embryonic mesenchymal cells share the potential for smooth muscle differentiation: myogenesis is controlled by the cell's shape." *Development* **126**(13): 3027-3033.

Zanier, ER, Fumagalli S, Perego C, Pischiutta F, De Simoni MG (2015). "Shape descriptors of the "never resting" microglia in three different acute brain injury models in mice." *Intensive care medicine experimental* **3**(1): 39.
Zhang, D, Kilian KA (2013). "The effect of mesenchymal stem cell shape on the maintenance of multipotency." *Biomaterials* **34**(16): 3962-3969.
Zhang, L, Kahn CJ, Chen HQ, Tran N, Wang X (2008). "Effect of uniaxial stretching on rat bone mesenchymal stem cell: orientation and expressions of collagen types I and III and tenascin-C." *Cell biology international* **32**(3): 344-352.

Table I. Changes in shape descriptors as function of biomaterial type, substrate concentration, time, and cyclic stretch

			Absolute Values				Value relative to 80 mg/ml collagen I sheets (%) **			
Effects associated with biomaterial type and coating		Nanoscale Stiffness	Roundness	Aspect Ratio	Circularity	Solidity	Roundness	Aspect Ratio	Circularity	Solidity
Compacted collagen I sheets	80 mg/ml concentration	10.2±0.8 kPa	0.398	3.19	0.35	0.72	100.0	100.0	100.0	100.0
Uncoated (thick) silicone sheets	762 µm thickness	903.2±18.8 kPa	0.465	2.24	0.32	0.77	116.8	70.04	93.55	**106.1**
Uncoated (thin) silicone sheets	127 µm thickness	185.8±14.2 kPa	0.524	2.39	0.30	0.75	**131.8**	74.71	**87.39**	104.6
Silicone sheets (thick) coated with:	fibronectin	811.0±14.7 kPa	0.476	2.16	0.48	0.75	119.6	67.66	137.9	104.2
Effects associated with biomechanical stimulation										
During 5 % stretch	collagen I sheets (80 mg/ml)		0.391	3.34	0.34	0.71	**98.18**	**104.6**	97.79	**98.81**
1h after 2.5 % cyclicyal stretch	collagen I sheets (80 mg/ml)	Day								
		4	0.438	2.89	0.37	0.73	110.1	90.49	107.9	101.8
		5	0.415	3.19	0.37	0.75	104.3	99.83	107.3	104.5
1h after 5 % cyclicyal stretch	collagen I sheets (80 mg/ml)	Day								
		4	0.438	2.97	0.37	0.75	110.0	92.89	107.3	103.7
		5	0.425	3.12	0.36	0.73	106.9	97.57	104.4	101.3

	Value relative to *cursive condition (%)*			
Effects of substrate concentration, thickness, and culture time	Roundness	Aspect Ratio	Circularity	Solidity
Effects of substrate concentration (160 relative to ***80*** mg/ml collagen I, on day 4)	**120.8**	**34.95**	**63.87**	**61.96**
Effects of substrate thickness (thin relative to ***thick*** silicone, on day 4)	112.8	106.7	93.41	98.60
Effects of time on 80 mg/ml collagen I sheets (day 5 relative to ***day 4***)	101.1	50.45	**107.3**	96.67
Effects of time on 160 mg/ml collagen I sheets (day 5 relative to **day 4**)	101.0	100.2	104.4	**103.8**
Effects of cyclic stretch amplitude and loading time				
Effects of cyclic stretch amplitude on 80 mg/ml collagen I sheets (5 % relative to ***2.5 %*** , on day 4)	99.93	102.7	104.7	101.9
Effects of cyclic stretch amplitude on 80 mg/ml collagen I sheets (5 % relative to ***2.5 %*** , on day 5)	102.5	97.74	97.33	96.93
Effects of cyclic stretch time on 80 mg/ml collagen I sheets (day 5 relative to ***day 4*** at 2.5 % amplitude)	**94.71**	**110.3**	99.41	102.6
Effects of cyclic stretch time on 80 mg/ml collagen I sheets (day 5 relative to ***day 4*** , at 5 % amplitude)	97.15	105.0	92.42	97.65

Green indicates relative increases, red relative decreases; maxima are in bold. For all given absolute values, the SEM was in the range of ±0.010 to ±0.001

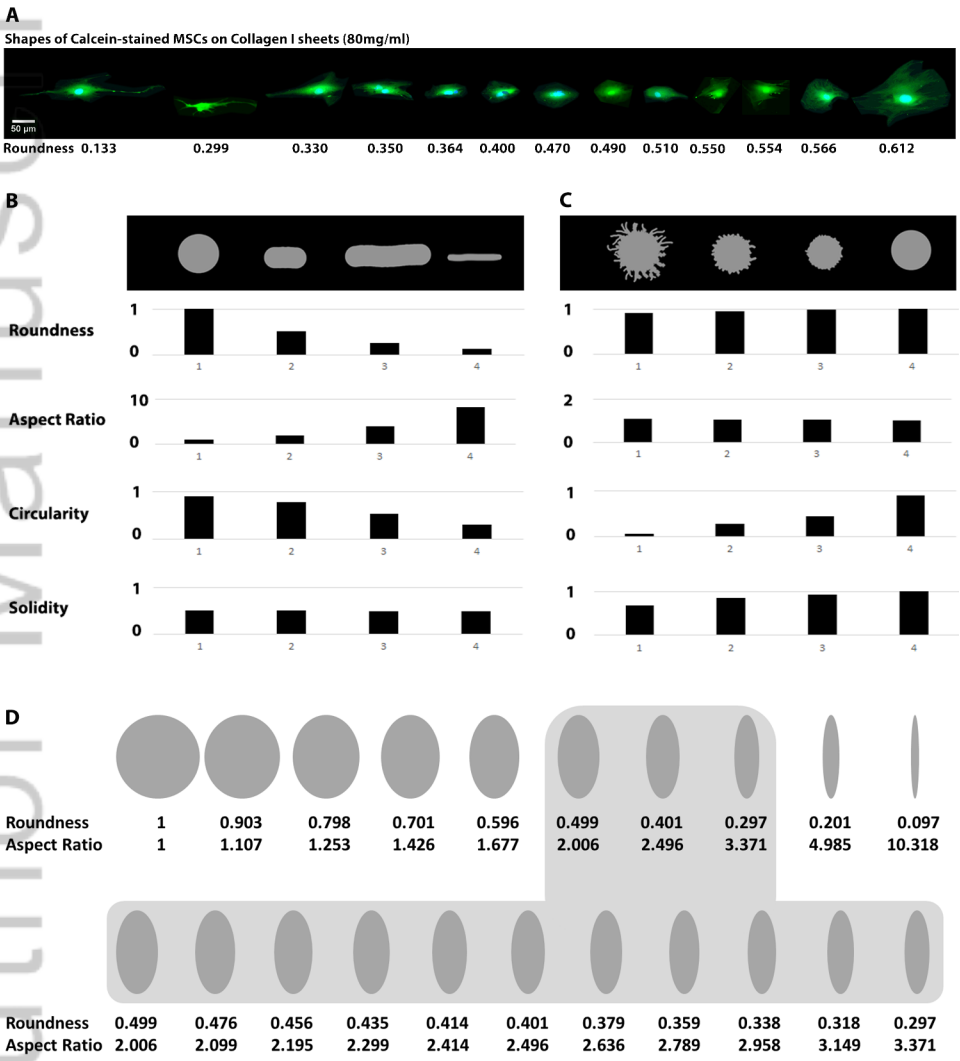

TERM_2263_F1.tif

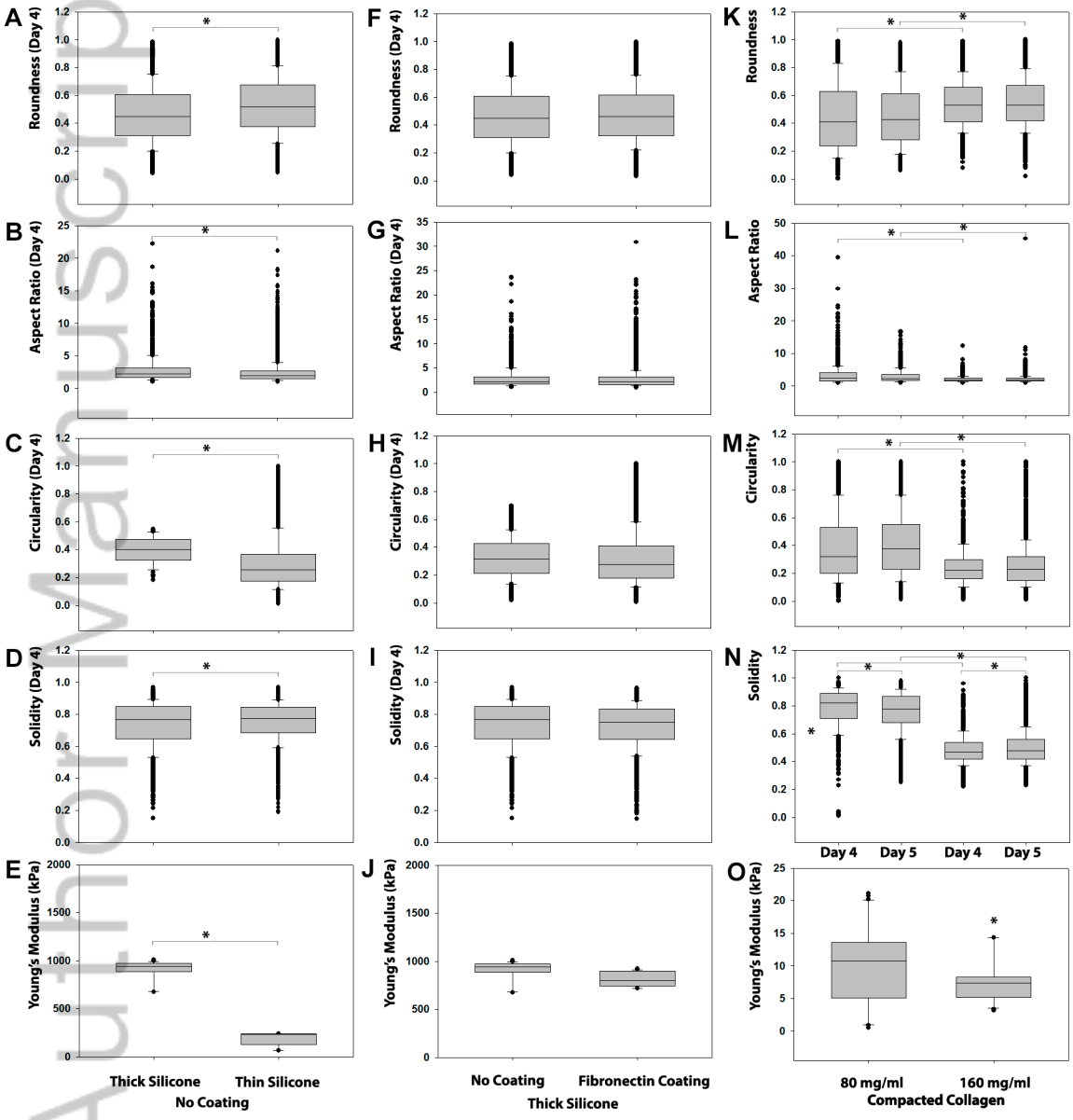

TERM_2263_F2.tif

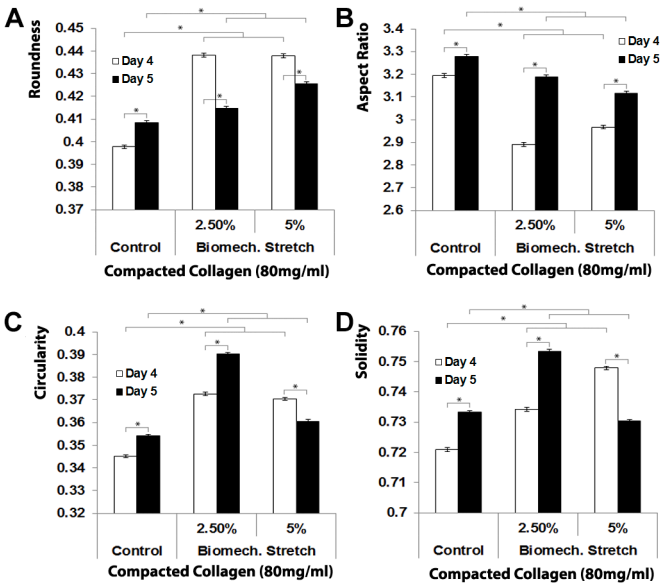

TERM_2263_F3.tif

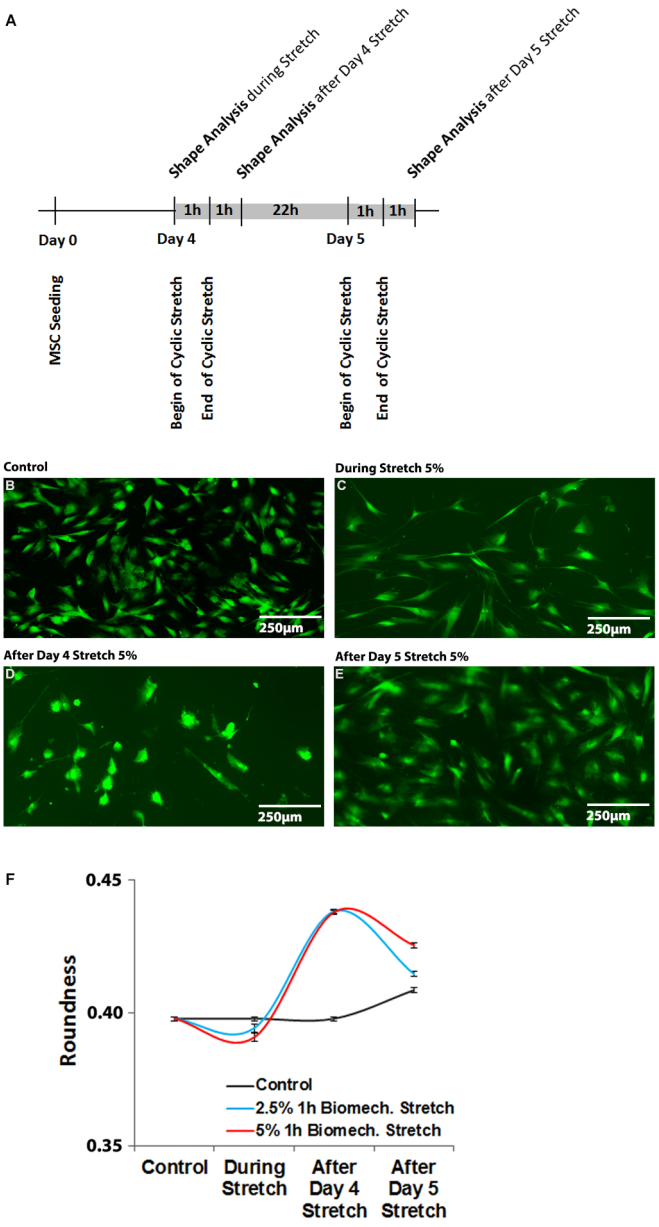

TERM_2263_F4.tif

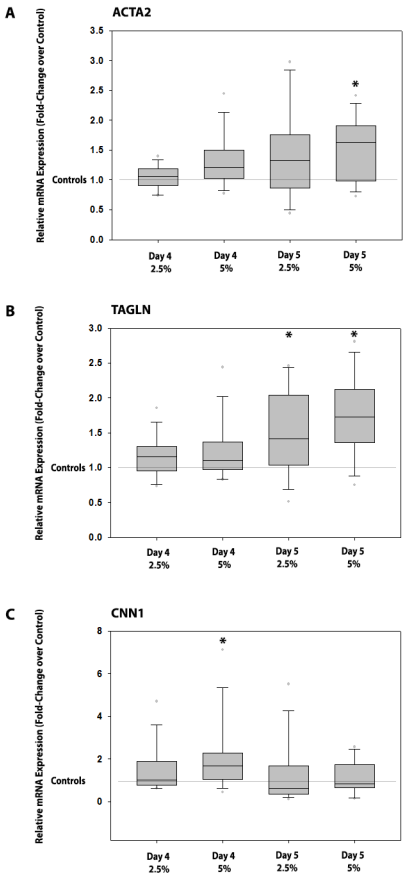

TERM_2263_F5.tif

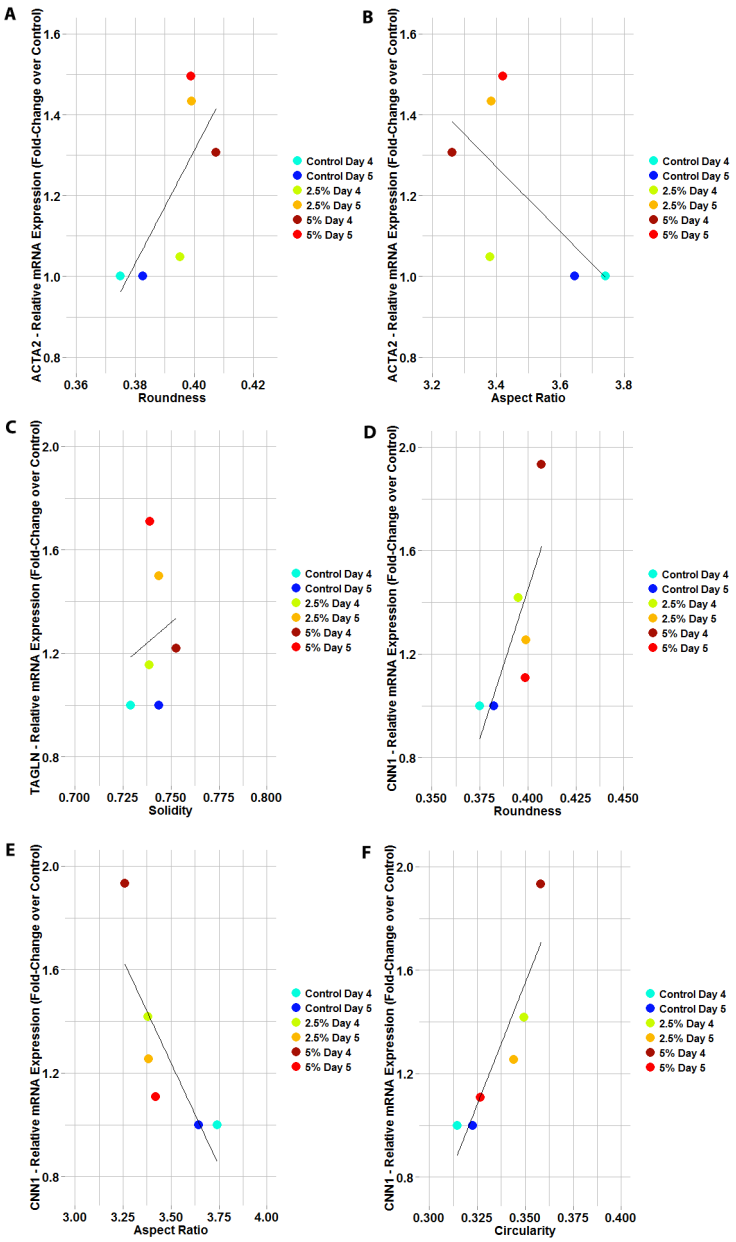

TERM_2263_F6.tif

Table I. Changes in shape descriptors as function of biomaterial type, substrate concentration, time, and cyclic stretch

			Absolute Values				Value relative to 80 mg/ml collagen I sheets (%) **			
Effects associated with biomaterial type and coating		Nanoscale Stiffness *	Roundness	Aspect Ratio	Circularity	Solidity	Roundness	Aspect Ratio	Circularity	Solidity
Compacted collagen I sheets	80 mg/ml concentration	10.2±0.8 kPa	0.398	3.19	0.35	0.72	100.0	100.0	100.0	100.0
Uncoated (thick) silicone sheets	762 µm thickness	903.2±18.8 kPa	0.465	2.24	0.32	0.77	116.8	70.04	93.55	**106.1**
Uncoated (thin) silicone sheets	127 µm thickness	185.8±14.2 kPa	0.524	2.39	0.30	0.75	**131.8**	74.71	**87.39**	104.6
Silicone sheets (thick) coated with:	collagen I (PureCol)	782.2±21.5 kPa	0.488	2.12	0.49	0.76	122.6	**66.41**	**141.3**	105.1
	collagen I (Roche)	756.9±19.7 kPa	0.462	2.27	0.46	0.74	116.1	70.98	133.8	102.8
	fibronectin	811.0±14.7 kPa	0.476	2.16	0.48	0.75	119.6	67.66	137.9	104.2
	laminin-511		0.471	2.19	0.47	0.76	118.3	68.60	136.4	106.0
Effects associated with biomechanical stimulation										
During 5 % stretch	collagen I sheets (80 mg/ml)		0.391	3.34	0.34	0.71	**98.18**	**104.6**	97.79	**98.81**
1h after 2.5 % cyclical stretch	collagen I sheets (80 mg/ml)	Day								
		4	0.438	2.89	0.37	0.73	110.1	90.49	107.9	101.8
		5	0.415	3.19	0.37	0.75	104.3	99.83	107.3	104.5
1h after 5 % cyclical stretch	collagen I sheets (80 mg/ml)	Day								
		4	0.438	2.97	0.37	0.75	110.0	92.89	107.3	103.7
		5	0.425	3.12	0.36	0.73	106.9	97.57	104.4	101.3

	Value relative to *cursive condition (%)*			
Effects of substrate concentration, thickness, and culture time	Roundness	Aspect Ratio	Circularity	Solidity
Effects of substrate concentration (160 relative to ***80*** mg/ml collagen I, on day 4)	**120.8**	**34.95**	**63.87**	**61.96**
Effects of substrate thickness (thin relative to ***thick*** silicone, on day 4)	112.8	106.7	93.41	98.60
Effects of time on 80 mg/ml collagen I sheets (day 5 relative to ***day 4***)	101.1	50.45	**107.3**	96.67
Effects of time on 160 mg/ml collagen I sheets (day 5 relative to **day 4**)	101.0	100.2	104.4	**103.8**
Effects of cyclic stretch amplitude and loading time				
Effects of cyclic stretch amplitude on 80 mg/ml collagen I sheets (5 % relative to ***2.5 %*** , on day 4)	99.93	102.7	104.7	101.9
Effects of cyclic stretch amplitude on 80 mg/ml collagen I sheets (5 % relative to ***2.5 %*** , on day 5)	102.5	97.74	97.33	96.93
Effects of cyclic stretch time on 80 mg/ml collagen I sheets (day 5 relative to ***day 4*** at 2.5 % amplitude)	**94.71**	**110.3**	99.41	102.6
Effects of cyclic stretch time on 80 mg/ml collagen I sheets (day 5 relative to ***day 4*** , at 5 % amplitude)	97.15	105.0	92.42	97.65

Green indicates relative increases, red relative decreases; maxima are in bold. For all given absolute values, the SEM was in the range of ±0.010 to ±0.001